

TOPBP1^{Dpb11} plays a conserved role in homologous recombination DNA repair through the coordinated recruitment of 53BP1^{Rad9}

Yi Liu,^{1*} José Renato Cussiol,^{1*} Diego Dibitetto,^{3*} Jennie Rae Sims,¹ Shyam Twayana,³ Robert Samuel Weiss,² Raimundo Freire,⁴ Federica Marini,³ Achille Pellicoli,^{3**} and Marcus Bustamante Smolka^{1**}

¹Department of Molecular Biology and Genetics, Weill Institute for Cell and Molecular Biology, Cornell University, Ithaca, NY 14853

²Department of Biomedical Sciences, Cornell University, Ithaca, NY 14853

³Department of Biosciences, University of Milan, 20133 Milan, Italy

⁴Unidad de Investigación, Hospital Universitario de Canarias, Instituto de Tecnologías Biomedicas, 38320 Tenerife, Spain

Genome maintenance and cancer suppression require homologous recombination (HR) DNA repair. In yeast and mammals, the scaffold protein TOPBP1^{Dpb11} has been implicated in HR, although its precise function and mechanism of action remain elusive. In this study, we show that yeast Dpb11 plays an antagonistic role in recombination control through regulated protein interactions. Dpb11 mediates opposing roles in DNA end resection by coordinating both the stabilization and exclusion of Rad9 from DNA lesions. The Mec1 kinase promotes the pro-resection function of Dpb11 by mediating its interaction with the Slx4 scaffold. Human TOPBP1^{Dpb11} engages in interactions with the anti-resection factor 53BP1 and the pro-resection factor BRCA1, suggesting that TOPBP1 also mediates opposing functions in HR control. Hyperstabilization of the 53BP1–TOPBP1 interaction enhances the recruitment of 53BP1 to nuclear foci in the S phase, resulting in impaired HR and the accumulation of chromosomal aberrations. Our results support a model in which TOPBP1^{Dpb11} plays a conserved role in mediating a phosphoregulated circuitry for the control of recombinational DNA repair.

Introduction

The proper repair of double-strand breaks (DSBs) that occur during DNA replication is heavily dependent on error-free homologous recombination (HR; Schwartz and Heyer, 2011; Heyer, 2015). However, DSBs may also be repaired by the direct ligation of DNA ends through nonhomologous end joining (NHEJ). Because of the risk of ligating wrong ends and/or deleting DNA sequences, NHEJ is considered to be an error-prone repair mechanism. During DNA replication, NHEJ repair has been proposed to be deleterious because of the intrinsic increased incidence of breaks, especially of one-ended DSBs, whose inappropriate joining could lead to dicentric chromosomes that initiate break–fusion cycles and complex chromosome rearrangements (Gaillard et al., 2015; Gelot et al., 2015). Therefore, NHEJ-mediated mutagenic repair is believed to be

a major contributor to genomic instabilities and tumorigenesis that arise when the HR machinery is defective (Deng and Wang, 2003; Prakash et al., 2015). The ability of cells to inhibit NHEJ and promote error-free HR repair during DNA replication is essential for genome integrity.

A critical step in regulating the choice of HR or NHEJ for repair is the control of 5′-to-3′ nucleolytic processing of DNA ends (also known as resection), as the formation of long 3′ single-stranded DNA (ssDNA) tails naturally promotes HR while preventing NHEJ (Chapman et al., 2012b; Prakash et al., 2015). 53BP1 is a scaffolding protein that plays a major role in limiting resection (Bothmer et al., 2010; Bunting et al., 2010). Although the mechanism by which 53BP1 limits resection remains incompletely understood, it involves the 53BP1-dependent recruitment of additional anti-resection factors such as RIF1 (Callen et al., 2013; Chapman et al., 2013; Di Virgilio et al., 2013; Escribano-Díaz et al., 2013; Zimmermann et al., 2013; Kumar and Cheok, 2014). On the other hand, in S phase, the tumor suppressor BRCA1 is proposed to play a pro-HR function by counteracting the recruitment of 53BP1 to

*Y. Liu, J.R. Cussiol, and D. Dibitetto contributed equally to this paper.

**A. Pellicoli and M.B. Smolka contributed equally to this paper.

Correspondence to Marcus Bustamante Smolka: mbs266@cornell.edu

Abbreviations used: 4OHT, 4-hydroxytomoxifen; BRCT, BRCA1 C terminus; ChIP, chromatin immunoprecipitation; CTR, constitutive TOPBP1-interacting region; DOX, doxycycline; DSB, double-strand break; HO, homothallic switching; HR, homologous recombination; HU, hydroxyurea; MBD, minimal multi-BRCT domain; MMS, methyl methanesulfonate; NHEJ, nonhomologous end joining; PARP, poly(ADP-ribose) polymerase; qPCR, quantitative PCR; RPA, replication protein A; SILAC, stable isotope labeling with amino acids in cell culture; SSA, single-strand annealing; ssDNA, single-stranded DNA; UDR, ubiquitination-dependent recruitment.

© 2017 Liu et al. This article is distributed under the terms of an Attribution–Noncommercial–Share Alike–No Mirror Sites license for the first six months after the publication date (see <http://www.rupress.org/terms/>). After six months it is available under a Creative Commons license (Attribution–Noncommercial–Share Alike 4.0 International license, as described at <https://creativecommons.org/licenses/by-nc-sa/4.0/>).



DSBs, therefore enabling resection (Bunting et al., 2010). This model is supported by genetic data in mice showing that the loss of 53BP1 suppresses embryonic lethality, genomic rearrangements, and tumorigenesis seen in mice lacking functional BRCA1 (Cao et al., 2009; Bouwman et al., 2010; Bunting et al., 2010; Prakash et al., 2015). DNA end resection is inhibited during the S phase in cells lacking BRCA1, and the increased recruitment of 53BP1 to replication-induced lesions results in increased chromosomal aberrations, which has been suggested to occur through mutagenic NHEJ repair (Bunting et al., 2010; Escribano-Díaz et al., 2013). Collectively, these observations support a model for repair pathway choice in which BRCA1 and 53BP1 compete for the sites of DNA lesions to promote HR or NHEJ. Despite strong genetic evidence supporting this model, it remains unclear exactly how 53BP1 promotes chromosomal instabilities upon BRCA1 dysfunction, as NHEJ is not the only potential source of mutagenic repair. For example, deregulated HR also has the potential to result in genomic instabilities, such as gross chromosomal rearrangements, caused by recombination between nonallelic sequences (Kolodner et al., 2002; Carr and Lambert, 2013). The role of BRCA1 in suppressing genomic instability during DNA replication may be dependent not only on counteracting 53BP1-mediated NHEJ, but also on ensuring that HR is properly executed for error-free repair. Although several mechanisms have been proposed to explain how the competition between BRCA1 and 53BP1 for DNA lesions is regulated (Kakarougkas et al., 2013; Tang et al., 2013; Orthwein et al., 2015; Zhang et al., 2016), the molecular mechanism by which BRCA1 is able to efficiently counteract 53BP1 during replication stress to favor DNA end resection remains incompletely understood.

Although many aspects of mammalian DNA repair are conserved in budding yeast, it remains unknown whether key mechanisms of HR control and DNA repair pathway choice are also conserved. Notably, a clear sequence homologue or a functional analogue of BRCA1 has not been identified in fungi. However, the 53BP1 orthologue Rad9 has been shown to play a conserved role in blocking resection (Lazzaro et al., 2008; Clerici et al., 2014; Ferrari et al., 2015). Cells lacking *RAD9* resect DSBs faster and more extensively (Lazzaro et al., 2008; Chen et al., 2012; Clerici et al., 2014). Of importance, it was recently proposed that a complex formed by the DNA repair scaffolds Slx4 and Rtt107 is able to counteract the engagement of Rad9 at replication-induced lesions to dampen DNA damage checkpoint signaling (Ohouo et al., 2013). Given the roles of Rad9 in blocking resection, we predicted that the ability of the Slx4–Rtt107 complex to counteract Rad9 recruitment to DNA lesions would help avert the block, therefore promoting resection. Indeed, recent work presented experimental evidence that the Slx4–Rtt107 complex favors resection of DSBs (Dibitetto et al., 2016).

Mammalian TOPBP1^{Dpb11} is an essential scaffolding protein that plays evolutionarily conserved roles in the initiation of DNA replication and activation of DNA damage checkpoint signaling (Tanaka et al., 2007; Zegerman and Diffley, 2007; Navadgi-Patil and Burgers, 2008; Puddu et al., 2008; Boos et al., 2011; Pfander and Diffley, 2011). TOPBP1^{Dpb11} is comprised of multiple BRCA1 C terminus (BRCT) domains (nine in humans and four in yeast), which are protein-interacting modules that often recognize phosphorylated motifs (Manke et al., 2003; Rodriguez et al., 2003; Yu et al., 2003). TOPBP1^{Dpb11} recognizes phosphoproteins to assemble the multisubunit

complexes required for replication initiation or checkpoint activation (Tak et al., 2006; Zegerman and Diffley, 2007; Boos et al., 2011; Pfander and Diffley, 2011). Although TOPBP1 has been implicated in HR repair (Morishima et al., 2007; Germann et al., 2011; Liu and Smolka, 2016; Moudry et al., 2016), its precise role and mode of action remain largely elusive. In this study, we show that in budding yeast, Dpb11 plays a decisive role in the control of DNA end resection, the first key step in HR, by mediating a competition between the anti-resection protein Rad9 and the pro-resection scaffolds Slx4–Rtt107 for DNA lesions. In humans, we find that TOPBP1 coordinates the recruitment of 53BP1 via a physical interaction that appears to be mutually exclusive with that of the pro-HR factor BRCA1. Our results support a model in which TOPBP1^{Dpb11} controls the mutually exclusive engagement of antagonistic regulators of recombinational DNA repair for the proper maintenance of genome integrity.

Results

BRCT domains of Dpb11 mediate mutually antagonistic functions in DNA end resection

In budding yeast, Dpb11 has been shown to recruit Rad9 to the 9-1-1 clamp (composed of Ddc1–Mec3–Rad17 in budding yeast and RAD9–HUS1–RAD1 in mammals) loaded at DNA lesions to promote activation of the DNA damage checkpoint (Fig. 1 A; Granata et al., 2010; Pfander and Diffley, 2011; Wang et al., 2012; Abreu et al., 2013). Because Rad9 and its human orthologue 53BP1 have both been shown to block DNA end resection, we hypothesized that the role of Dpb11 in mediating the recruitment of Rad9 to DNA breaks plays a decisive role in resection control and HR-mediated DNA repair. To test this, we fused BRCT domains 3/4 of Dpb11 with full-length Rad9 (Fig. 1 B), with the expectation that this chimera would hyperstabilize Rad9 at DNA lesions and block resection. Using a system to induce a persistent DSB at the mating-type (MAT) locus through the overexpression of homothallic switching (HO) endonuclease (White and Haber, 1990; Lee et al., 1998), we found that the Dpb11^{BRCT3/4}–Rad9 chimera (hereafter referred to as “BRCT3/4–Rad9”) is robustly detected at 0.15 kb from the break site using chromatin immunoprecipitation (ChIP)–quantitative PCR (qPCR; Fig. 1 C). Of importance, a point mutation corresponding to K544A in Dpb11, known to disrupt the ability of BRCT3/4 to recognize phosphorylated 9-1-1, prevents the stabilization of BRCT3/4–Rad9 near the site of DSB (Fig. 1 C). Taking advantage of this system, we assessed the effect of Dpb11-mediated Rad9 hyperstabilization on resected DNA ends using an assay to monitor the accumulation of ssDNA flanking an irreparable HO-induced DSB site (Ferrari et al., 2015; Dibitetto et al., 2016). Although we did not observe an impact on resection at 0.15 kb from the break, resection is significantly inhibited at 1.4 kb and severely blocked at 4.8 kb from the break site upon expression of the BRCT3/4–Rad9 chimera (Fig. 1 D). The K544A mutation that impairs BRCT3/4 fully restored resection, arguing that the ability of Dpb11 to bridge Rad9 to the 9-1-1 complex is crucial to inhibit long-range resection. Consistent with this model, expression of the BRCT3/4–Rad9 chimera strongly impaired the repair of one HO cut through a single-strand annealing (SSA) mechanism that relies on extensive resection (Fig. 1, E–G).

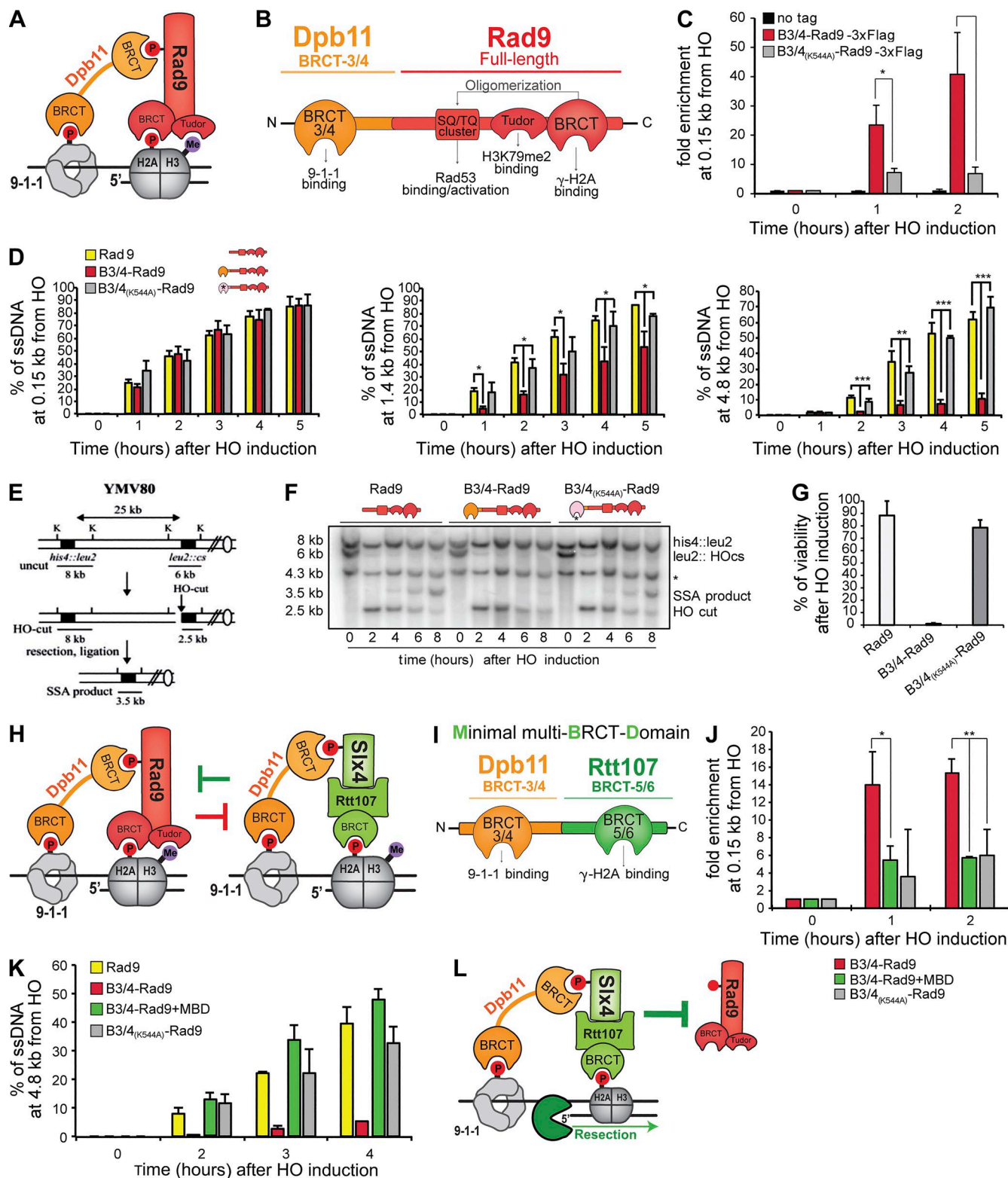


Figure 1. **A competition-based mechanism for the modulation of Rad9 recruitment and DNA end resection via Dpb11 BRCT domains.** (A) Working model for the role of Dpb11 in the recruitment of Rad9 to the 5' recessed end of a DNA lesion. (B) Schematic illustration of the BRCT3/4-Rad9 chimera. (C) ChIP-qPCR analysis showing the recruitment of BRCT3/4-Rad9 to an HO-induced DSB site. JKM139-derivative strains expressing the indicated chimera proteins or an untagged Rad9 control were arrested with nocodazole, and HO endonuclease expression was then induced for the indicated time to trigger an irreparable DSB on chromosome III. (D) HO-induced DSB resection analysis by qPCR in nocodazole-arrested JKM139-derivative strains expressing the indicated Rad9 constructs. (E) Schematic illustration for the SSA repair assay measurement. The graph shows the YMV80 chromosome III region containing an HO cut site. The DNA probe hybridizes to sequences within the indicated black boxes. K, *KpnI* cut site. (F) Successful SSA requires 25-kb resection and can be monitored by the appearance of a 3.5-kb SSA product using Southern blot analysis (shown here), where an *ATG5* (uncut locus on chromosome XVI) probe (marked by an asterisk) was used to normalize the signals. HOcs, HO cut site. (G) Exponentially growing YMV80-derivative strains of each

We have recently proposed a model in which Dpb11 also coordinates the controlled disengagement of Rad9 from lesions for dampening checkpoint signaling (Fig. 1 H; Ohouo et al., 2013; Cussiol et al., 2015). In this model, the Slx4–Rtt107 scaffolding complex competes with Rad9 for Dpb11 interaction, ultimately preventing Rad9 from stabilizing at DNA lesions. We hypothesized that this competition mechanism is also crucial to control the roles of Rad9 in DNA repair and could provide the molecular basis to understand how 53BP1 recruitment is regulated in mammals. We predicted that a fusion of the Slx4–Rtt107 complex with Dpb11 BRCT3/4 should be able to antagonize the BRCT3/4–Rad9 chimera and restore resection. We have previously shown that a fusion of Dpb11 BRCT3/4 with Rtt107 BRCT5/6 (referred as the minimal multi-BRCT domain [MBD] module; Fig. 1 I) mimics the role of the Dpb11–Slx4–Rtt107 complex in checkpoint dampening (Cussiol et al., 2015). Here, we found that expression of MBD prevents hyperstabilization of the BRCT3/4–Rad9 chimera at DSBs (Fig. 1 J) and, strikingly, fully suppresses the resection block induced by BRCT3/4–Rad9 (Fig. 1 K). Collectively, these results are consistent with a model in which Dpb11 plays mutually antagonistic roles in resection by coordinating the stabilization as well as the exclusion of Rad9 from DNA lesions (Fig. 1, H and L).

Dpb11-mediated recruitment of Rad9 impairs HR-mediated repair in response to replication stress

Slx4 and Rtt107 have been shown to be particularly important in the response to methyl methanesulfonate (MMS)–induced replication stress (Fricke and Brill, 2003; Chin et al., 2006; Roberts et al., 2006; Ohouo et al., 2010). We therefore asked whether the BRCT3/4–Rad9 chimera also impairs the control of resection and HR-mediated repair in cells treated with MMS, a DNA alkylating agent that blocks replication fork progression. Although MMS treatment resulted in the formation of multiple replication protein A (RPA) foci, an indirect marker of ssDNA exposure, in cells expressing the mutated BRCT3/4(K544A)–Rad9 chimera, expression of the chimera BRCT3/4–Rad9 bearing functional BRCT3/4 prevented most cells from accumulating multiple RPA foci (Fig. 2, A and B), consistent with the lower accumulation of ssDNA at replication forks likely caused by the inhibition of DNA end resection. This defect in RPA foci formation is accompanied by a severe reduction in foci formation of the HR protein Rad52 (Fig. 2, C and D), pointing to an impairment of HR-mediated repair. Of note, coexpression of the MBD chimera restored the accumulation of RPA and Rad52 foci in cells expressing the BRCT3/4–Rad9 chimera. These results support that Dpb11-mediated recruitment of Rad9 also plays an important role in coordinating DNA end resection and HR repair in the response to replication blocks. MBD coexpression or K544A mutation in the BRCT3/4–Rad9 chimera were

also sufficient to rescue BRCT3/4–Rad9–induced MMS sensitivity (Fig. 2, E and F). Furthermore, expression of BRCT3/4–Rad9 led to hyperactivation of the checkpoint effector kinase Rad53 in cells treated with MMS as evaluated by the mobility shift of Rad53 (Fig. 2 G), consistent with the Dpb11-mediated function of Rad9 in promoting checkpoint signaling. This aberrant Rad53 hyperphosphorylation, as well as the appearance of a hypershifted form of BRCT3/4–Rad9, was suppressed by the coexpression of MBD, which is in agreement with the reduced binding of BRCT3/4–Rad9 nearby an HO-induced DSB upon MBD expression. These data again reinforce the competition-based model in which Dpb11 regulates HR-mediated repair by coordinating the mutually exclusive recruitment of Slx4 and Rad9 and reveal that Dpb11 plays antagonistic roles in HR-mediated repair also in the context of replication stress.

The Mec1 kinase promotes resection via phosphorylation of Slx4

According to our model, the control of Dpb11 interactions with Slx4 or Rad9 is expected to play a key role in the control of DNA end resection. Therefore, the decision to specifically stabilize the Dpb11–Slx4 interaction should be the distinguishing molecular event that transitions Dpb11's function from blocking resection to favoring resection. Because interactions of Dpb11 with Slx4 and Rad9 are both dependent on CDK (Pfander and Diffley, 2011; Wang et al., 2012; Ohouo et al., 2013; Gritenaite et al., 2014), we reasoned that CDK activity is unlikely to be the discerning molecular event that commands the choice of Slx4 versus Rad9 stabilization at DNA lesions. Previously, we have shown that the Dpb11–Slx4 interaction is strongly induced by DNA damage and requires the Mec1 kinase (Ohouo et al., 2010). Here, we show that Mec1 is specifically required to enhance the Dpb11–Slx4 interaction but plays a minor role in the control of the Dpb11–Rad9 interaction (Fig. 3, A and B). During MMS-induced replication stress or phleomycin-induced DSBs in the G2/M transition, the Dpb11–Slx4 interaction was largely dependent on Mec1. However, we observed only a slight reduction of the Dpb11–Rad9 interaction upon deletion of *MEC1*. These results are consistent with the model in which Mec1 signaling plays a decisive role in promoting DNA end resection via Slx4 phosphorylation. To test this, we analyzed resection in the *slx4-7MUT* mutant bearing mutation of seven Mec1 consensus phosphorylation sites, which we have previously shown to specifically impair binding to Dpb11 but not to impair binding to other Slx4-interacting proteins (Ohouo et al., 2010, 2013). As shown in Fig. 3 C, resection in the *slx4-7MUT* mutant was impaired, close to the level observed in cells lacking *SLX4*. We therefore propose a model in which Mec1 signaling, through the formation of a Dpb11–Slx4–Rtt107 complex, counteracts a resection block imposed by the Dpb11–Rad9 complex (Fig. 3 D).

indicated genotype were plated on YP + glucose and YP + galactose and incubated at 28°C for 3 d. The viability values were obtained by dividing the number of colonies grown on YP + galactose by the number of colonies growing on YP + glucose. Plotted values are the means of at least two independent experiments \pm SD. (H) A working model for the role of the Dpb11–Slx4–Rtt107 complex in antagonizing Rad9 recruitment at lesion sites. Me, methylation. (I) Schematic illustration of the MBD chimera. (J) ChIP-qPCR analysis of BRCT3/4–Rad9 or BRCT3/4(K544A)–Rad9 recruitment to one irreparable HO cut in nocodazole-arrested JKM139-derivative strains expressing the indicated chimeric proteins. (K) DSB resection analysis by qPCR to determine the effect of MBD expression on resection efficiency in nocodazole-arrested JKM139-derivative strains expressing Rad9, BRCT3/4–Rad9, or BRCT3/4(K544A)–Rad9. (C, D, J, and K) Graphs are plotted using means \pm SEM from two (K), three (D and J), or four (C) independent experiments. P-values were determined based on a one-tailed Student's *t* test. *, $P < 0.05$; **, $P < 0.01$; ***, $P < 0.001$. B3/4, BRCT3/4. (L) A working model for the role of the Slx4–Rtt107 complex in counteracting the Dpb11-mediated recruitment of Rad9 to promote DNA end resection. For the experiments in this figure, BRCT3/4–RAD9 and MBD chimeras were integrated into the RAD9 and SLX4 loci, respectively. P, phosphorylation.

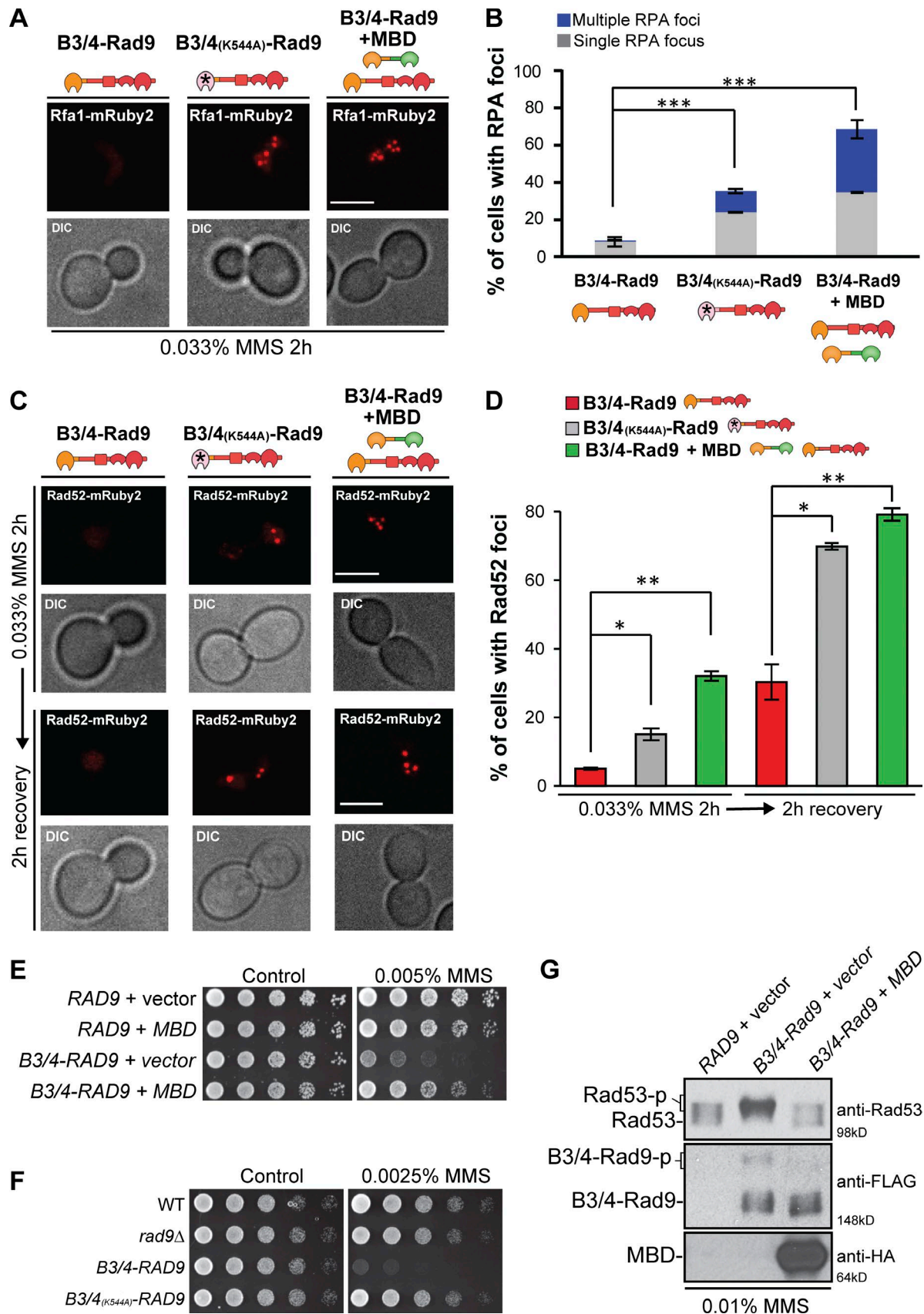


Figure 2. Dpb11-mediated hyperstabilization of Rad9 impairs proper HR repair of replication-induced lesions. (A and B) Rfa1-mRuby2 foci were quantified in MMS-treated cells expressing either the BRCT3/4-Rad9 chimera or the mutated BRCT3/4(K544A)-Rad9 chimera or coexpressing the MBD and BRCT3/4-Rad9 chimeras. Representative images are shown in A. Percentages of cells with one Rfa1 focus or with multiple Rfa1 foci were quantified

Proteomic analysis in human cells reveals TOPBP1 interactions with antagonistic repair factors

Based on our findings in yeast, we speculated that TOPBP1 also plays a role in coordinating the recruitment of antagonistic factors for the proper control of DNA repair in mammals. Previous studies revealed that TOPBP1 indeed interacts with 53BP1 as well as with a range of pro-HR factors, including BRCA1-associated proteins (Yamane et al., 2002; Greenberg et al., 2006; Morishima et al., 2007; Yoo et al., 2009; Cescutti et al., 2010). We reasoned that TOPBP1 interactions specifically induced by replication stress should reveal pro-HR functions for TOPBP1. We therefore performed an unbiased mass spectrometry analysis to define the network of TOPBP1 interactions in cells either treated with hydroxyurea (HU), to induce replication stress, or with nocodazole, to reveal interactions that are independent of replication stress (Fig. 4 A and Tables S3 and S4). Next, we measured the changes of the identified interactions by directly comparing cells treated with HU or nocodazole to specifically reveal interactions induced by replication stress (Fig. 4 B and Table S5). Although most interactions did not display major changes in our comparison (Fig. 4 B), the interaction of human TOPBP1 with a pro-HR factor, BRCA1, is strongly induced by replication stress (Fig. 4 B), similar to what we previously observed for yeast Dpb11 (Ohouo et al., 2010). Of interest, the interaction of TOPBP1 with 53BP1 is reduced under replication stress (Fig. 4, B and C), suggesting that the interactions of TOPBP1 with BRCA1 and 53BP1 are mutually exclusive. Similar results were observed when comparing untreated asynchronous cells with HU-treated cells (Fig. S1 C), further suggesting that the TOPBP1–53BP1 interaction is largely constitutive and is counteracted upon replication stress. This notion is further supported by the findings that both of these interactions are disrupted by mutations that impair the BRCT1/2 or BRCT4/5 domains of TOPBP1 (Fig. 4 D) and that BRCA1 could not be detected in a 53BP1 immunoprecipitation and vice versa (Fig. S1, A and B). Because 53BP1 and BRCA1 localize to sites of DNA lesions in a mutually exclusive manner (Chapman et al., 2012a) and have been proposed to compete for DNA lesions to dictate repair pathway choice (Cao et al., 2009; Bouwman et al., 2010; Bunting et al., 2010; Chapman et al., 2012a), our findings suggest that TOPBP1 could be the mediator of such competition, similar to the role of Dpb11 in coordinating the competition between Rad9 and Slx4 in yeast. Also similar to the yeast model, the ATR kinase plays an important role in promoting the interaction of TOPBP1 with a pro-HR factor (in this case, BRCA1) but is not required for enhancing the TOPBP1–53BP1 interaction (Fig. 4 E). Overall, these findings are consistent with a model in which yeast Dpb11 and mammalian TOPBP1 have roles in coordinating the action of antagonistic repair factors (Fig. 4 F).

Hyperstabilization of the TOPBP1–53BP1 interaction promotes 53BP1 recruitment to nuclear foci in the S phase

Based on our findings in yeast, we hypothesized that human TOPBP1 controls the recruitment of 53BP1 to DNA lesions under certain conditions and is important to mediate 53BP1-dependent DNA repair. To test this hypothesis, we engineered a system to stabilize the TOPBP1–53BP1 interaction. We were unable to generate a chimeric mammalian protein similar to the BRCT3/4–Rad9 fusion we generated in yeast because fusion proteins of 53BP1 with BRCT domains of TOPBP1 did not express in human cell lines. To circumvent this issue, we fused 53BP1 to a 120–amino acid region from the N-terminal domain of replication factor C subunit 1 (RFC1), which we found to constitutively interact with TOPBP1 (Fig. 4 B). Thus, by fusing the N terminus of RFC1 (hereafter referred to as the constitutive TOPBP1-interacting region [CTR]) to 53BP1 (Fig. 5 A), we reasoned that the interaction of this chimera with TOPBP1 would be stabilized and enhanced during replication stress. Indeed, the CTR–53BP1 chimeric protein displays enhanced interaction with TOPBP1 after HU treatment (Fig. 5 B). Strikingly, the CTR–53BP1 chimera forms significantly more nuclear foci compared with 53BP1 alone in cells progressing through the S phase after release from an HU-induced arrest (Fig. 5, C and D; and Fig. S2 A), suggesting the enhanced recruitment of CTR–53BP1 to replication-induced lesions.

Once recruited to the lesion site, 53BP1 promotes the recruitment of PTIP and RIF1, two proteins believed to function as effectors of NHEJ and/or as blockers of resection (Callen et al., 2013; Chapman et al., 2013; Di Virgilio et al., 2013; Escribano-Díaz et al., 2013; Feng et al., 2013; Zimmermann et al., 2013). To investigate whether the increased recruitment of CTR–53BP1 functionally impacts 53BP1-mediated DNA repair, we first monitored PTIP and RIF1 status. Interestingly, CTR–53BP1 pulled down more PTIP compared with 53BP1 alone, despite the relatively lower expression level of CTR–53BP1 (Fig. 5 B). In addition, although we were unable to monitor PTIP foci using available antibodies, we found that CTR–53BP1 induces a significant increase in the number of RIF1 foci in S-phase cells released from an HU arrest (Fig. 5, C and D; and Fig. S2 A). Because RIF1 and PTIP recruitment to DNA lesions is believed to require DNA damage–induced phosphorylation of 53BP1 (Munoz et al., 2007; Callen et al., 2013; Chapman et al., 2013; Di Virgilio et al., 2013; Escribano-Díaz et al., 2013; Zimmermann et al., 2013; Kumar and Cheok, 2014), our results strongly suggest that the enhanced interaction with TOPBP1 increases the engagement of CTR–53BP1 at sites of lesions, culminating in its phosphorylation and the subsequent increased recruitment of RIF1 and, likely, PTIP.

and plotted in B. More than 300 cells were scored per replicate. (C and D) Rad52-mRuby2 foci were quantified in cells expressing either BRCT3/4–Rad9 or the mutated BRCT3/4(K544A)–Rad9 chimera or coexpressing the MBD and BRCT3/4–Rad9 chimeras. Cells were analyzed after treatment with 0.033% MMS for 2 h or after recovery of cells for 2 h in fresh media after MMS treatment. Cells were evaluated based on the presence or the absence of Rad52-mRuby2 foci. More than 300 cells were scored per replicate. Representative images are shown in C. The percentage of cells with Rad52 foci were quantified and plotted in D. Bars, 5 μ m. DIC, differential interference contrast. (E) MMS sensitivity of wild-type cells expressing MBD and/or BRCT3/4–Rad9 from plasmids. Fourfold serial dilutions were spotted on SC-URA-TRP plates and grown for 2–3 d at 30°C. (F) MMS sensitivity of cells expressing either BRCT3/4–Rad9 or BRCT3/4(K544A)–Rad9 from the endogenous RAD9 locus. Fourfold serial dilutions were spotted on YPD plates and grown for 2–3 d at 30°C. WT, wild type. (G) Immunoblots showing the phosphorylation status of Rad53 and BRCT3/4–Rad9 in cells expressing Rad9 or BRCT3/4–Rad9 or coexpressing BRCT3/4–Rad9 with MBD. The Rad9 fusions were integrated at the RAD9 locus and MBD was expressed from a plasmid (pMBS910). For A–D, F, and G, the BRCT3/4–Rad9 chimera was integrated into the RAD9 locus. B3/4, BRCT3/4. Graphs are plotted using means \pm SEM from at least three independent experiments. P-values were determined based on a two-tailed Student's *t* test. *, $P < 0.05$; **, $P < 0.01$; ***, $P < 0.001$.

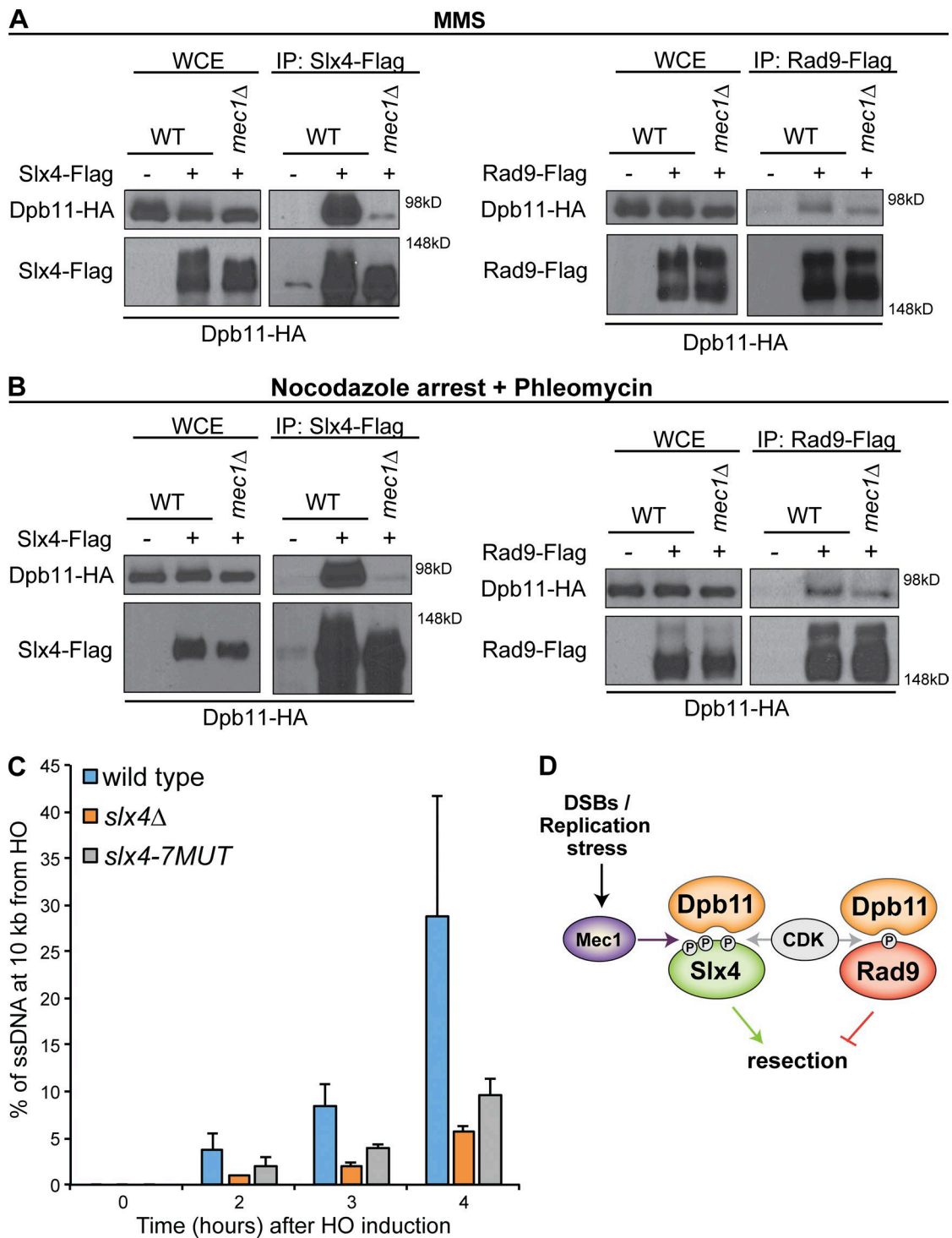


Figure 3. **Phosphorylation of Slx4 by Mec1 promotes DNA end resection.** (A) Coimmunoprecipitations of Dpb11 with Slx4 or Rad9 in wild-type (WT) or *mec1Δ* cells treated with 0.01% MMS for 3 h. (B) Coimmunoprecipitations of Dpb11 with Slx4 or Rad9 in wild-type or *mec1Δ* cells arrested with 7 μ g/ml nocodazole for 3 h followed by phleomycin treatment (40 μ g/ml) for 15 min in the continuous presence of nocodazole. IP, immunoprecipitation; WCE, whole cell extract. (C) DSB resection analysis by qPCR of the indicated nocodazole-arrested JKM139-derivative strains. The graph is plotted using means \pm SEM from two independent experiments. (D) A model for the role of Dpb11 in resection control via coordination of Slx4 and Rad9. P, phosphorylation.

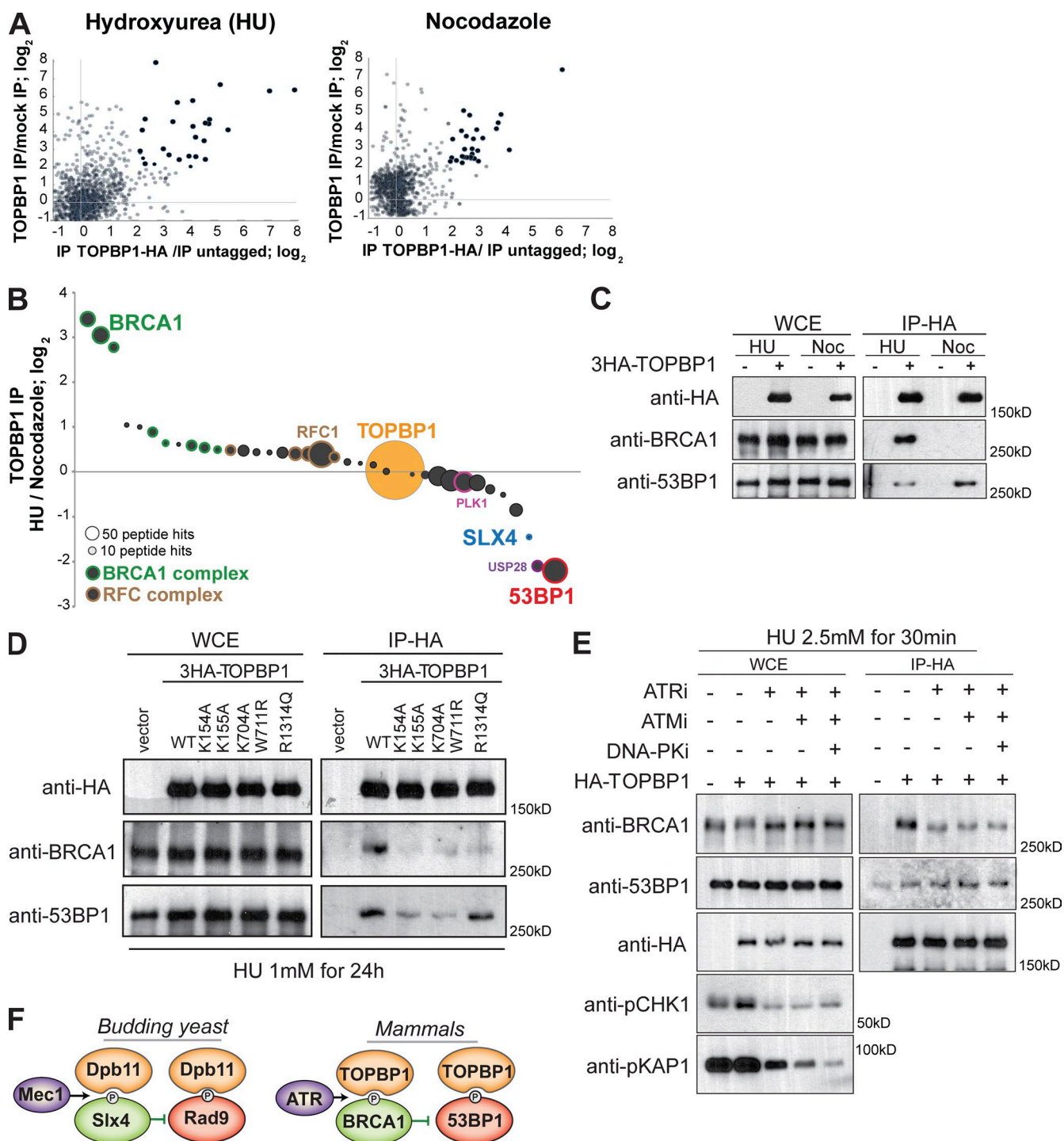


Figure 4. Proteomic analysis of TOPBP1 interactions modulated by replication stress. (A) Quantitative mass spectrometry analysis of TOPBP1 interactions in cells arrested with HU or nocodazole. HEK293T cells were grown in light and heavy SILAC media and were treated with 1 mM HU for 24 h to identify proteins that interact with TOPBP1 in response to replication stress. Two independent experiments were performed, one pulling down endogenous TOPBP1 with an anti-TOPBP1 antibody and the other pulling down overexpressed HA-TOPBP1 with anti-HA resin. Proteins with a TOPBP1 immunoprecipitation (IP)/mock immunoprecipitation ratio of >4 in both experiments were considered to be specific TOPBP1 interactors. Each dot in dark color represents an identified TOPBP1 interaction. Similar procedures were performed in cells treated with 100 ng/ml nocodazole for 14 h to define TOPBP1 interactions in G2/M. (B) Quantitative mass spectrometry analysis of changes in TOPBP1 interactions in HEK293T cells treated with 1 mM HU for 24 h (grown in light SILAC media) or treated with 100 ng/ml nocodazole for 14 h (grown in heavy SILAC media). (C) Coimmunoprecipitation of TOPBP1 with BRCA1 or 53BP1 in HEK293T cells treated with 1 mM HU or 100 ng/ml nocodazole (noc) as described in Fig. 3 A. (D) Coimmunoprecipitation experiment determining the contribution of each pair of BRCT domains in TOPBP1 for stabilizing interactions with BRCA1 and 53BP1. HEK293T cells were transfected with plasmids containing TOPBP1 (wild type and the following mutants: BRCT1: K154A and K155A; BRCT5: K704A and W711R; and BRCT7: R1314Q) or empty vector (see Table S2) and treated with 1 mM HU for 24 h. (E) Coimmunoprecipitation of TOPBP1 with BRCA1 or 53BP1 in the presence of ATR, ATM, or DNA-PK inhibitors. HEK293T cells transfected with HA-TOPBP1 were pretreated with ATR, ATM, or DNA-PK inhibitors for 45 min, followed by 30-min HU treatment in the presence of inhibitors. i, inhibitor; WCE, whole cell extract. (F) Depiction of an analogous mode of TOPBP1^{Dpb11} interactions with pro-HR (BRCA1 in humans and Slx4 in yeast) and anti-resection (53BP1^{Rad9}) factors. P, phosphorylation.

Hyperstabilization of the TOPBP1–53BP1 interaction impairs HR-mediated repair and induces chromosomal aberrations

The foci formed by CTR-53BP1 colocalized with γ -H2AX and RIF1 but not with RPA or RAD51, two markers for HR (Fig. S2 B), suggesting that the chimera is engaging in RIF1-mediated DNA repair in a mutually exclusive manner with the HR machinery. We therefore hypothesized that expression of CTR-53BP1 would induce genomic instability by promoting mutagenic NHEJ repair and/or deregulating HR-mediated repair. Indeed, we observed a significant increase in the number of chromosomal aberrations induced by the expression of CTR-53BP1, but not by the expression of ectopic 53BP1, in response to fork collapse induced by a combination of poly(ADP-ribose) polymerase (PARP) inhibitor (AZD2461) and ATR inhibitor (VE-821; Fig. 5 E). We also generated HEK293 cells with a stably integrated CTR-53BP1 whose expression is induced by doxycycline (DOX; Fig. 5 F and Fig. S3, A and B). In these cells, DOX treatment led to growth sensitivity (Fig. S3 C) and a striking accumulation of chromosomal aberrations, especially radial chromosomes, upon PARP inhibition (Fig. 5, G and H). We could observe some radials in these cells even in the absence of DOX (Fig. 5 H), which we attributed to a minor leakage expression of CTR-53BP1 in the absence of DOX (Fig. S3 A). Of importance, we note that overexpression of 53BP1 had only a minor impact in the cells we used. Despite ectopic 53BP1 being expressed at least five times more than CTR-53BP1 (Figs. 5 B and S4 B), overexpression of 53BP1 did not result in a significant increase in chromosomal aberrations (Fig. 5 E). Collectively, these findings support a model in which TOPBP1 mediates the recruitment of 53BP1 to DNA lesions to promote 53BP1-dependent genomic instability.

Consistent with the model that the TOPBP1–53BP1 interaction counteracts HR-mediated DNA repair, we observed that the expression of CTR-53BP1 reduced HR repair in the DR-GFP system (Fig. 5 I), a commonly used assay to test HR in human cells (Gunn and Stark, 2012). Again, the overexpression of 53BP1 had only a minor effect in inhibiting HR (Fig. S4, A and B), further consistent with the model that interaction of 53BP1 with TOPBP1 is important to stabilize 53BP1 at DNA lesions and to counteract HR-mediated repair. Expression of CTR-53BP1 bearing mutations in the tudor or ubiquitination-dependent recruitment (UDR) domains, which are important for the ability of 53BP1 to localize to sites of DNA lesions, also failed to reduce HR repair in the DR-GFP system (Fig. S4, A and B), supporting the claim that the ability of CTR-53BP1 to counteract HR requires recruitment to chromatin as well as TOPBP1 binding. As we observed in yeast, our results suggest that this effect is associated with a 53BP1-mediated block in DNA end resection. Although assays to measure DNA end resection in mammalian cells are not as well established as in yeast, we were able to observe a significant reduction in SSA repair (Fig. 5 J) through an assay that relies on extensive resection (Gunn and Stark, 2012) and a mild, but consistent, reduction in DNA end resection next to a DSB that was induced through the ER–AsiSI system (Figs. 5 K and S4 C; Iacovoni et al., 2010; Zhou et al., 2014). Finally, we noticed that the ability of CTR-53BP1 to induce chromosomal aberrations and impair HR-mediated repair was stronger upon siRNA-mediated knockdown of BRCA1 (Fig. 5, L and M; and Fig. S5, A and B). Congruent with the idea that the anti-HR function of the TOPBP1–53BP1 interaction is being counteracted by BRCA1,

a partial reduction in BRCA1 abundance (Fig. S5 B) strongly induced chromosomal aberrations upon CTR-53BP1 expression. Overall, although further investigation will be necessary to understand how TOPBP1 controls recombinational DNA repair and repair pathway choice, the results presented here are consistent with a model in which TOPBP1 mediates the competition between 53BP1 and BRCA1 for DNA lesions. As shown in Fig. 5 N, we propose a working model where the ability of TOPBP1 to bind to 53BP1 is important to stabilize 53BP1 at DNA lesions. In cells lacking functional BRCA1, TOPBP1 would promote 53BP1-mediated genomic instability, possibly by blocking resection, impairing error-free HR-mediated repair, and promoting mutagenic NHEJ repair. In normal cells, ATR would play a role in preventing genomic instability by promoting the BRCA1–TOPBP1 interaction and counteracting the engagement of 53BP1 at DNA lesions.

Discussion

Maintenance of genome integrity during DNA replication heavily relies on HR-mediated DNA repair. In *BRCA1* mutated cells lacking a functional HR machinery, the scaffolding protein 53BP1 plays a key role in promoting replication stress-induced chromosomal aberrations. In the last 10 years, the discovery that BRCA1 and 53BP1 play antagonistic roles in the control of DNA end resection provided a mechanistic explanation for how the lack of BRCA1 results in 53BP1-mediated genomic instability. However, it remains incompletely understood how the engagement of BRCA1 and 53BP1 at DNA lesions is regulated and which molecular mechanisms govern a likely competition between these factors. In this study, we build on mechanistic work in yeast to propose a central and evolutionarily conserved role for the TOPBP1^{Dpb11} scaffold in controlling the engagement of pro- and anti-resection factors for DNA repair control. We provide evidence to support that interactions of Dpb11 with the Rad9 and Slx4–Rtt107 scaffolds define a key phosphoregulated molecular circuitry for resection control. We also provide initial evidence to support a model in which mammalian TOPBP1 mediates a similar system for DNA repair control via the coordinated engagement of 53BP1 and BRCA1.

Central to this circuitry for resection control is the ability of TOPBP1^{Dpb11} to function both as a scaffold as well as an activator of ATR^{Mec1}, therefore integrating the action of this kinase into resection control. In our proposed model depicted in Fig. 3 D for yeast, Dpb11 functions as a scaffolding module to stabilize pro- or anti-resection factors at DNA lesions, and activation of the Mec1 kinase plays a decisive role in shifting Dpb11's role from an inhibitor of resection (via the Dpb11–Rad9 complex) to a positive regulator of resection (via the Dpb11–Slx4–Rtt107 complex). Interestingly, when bound to Rad9, Dpb11 is also coordinating Mec1 signaling, but in this case, it is contributing to transduce Mec1 signaling toward Rad53 activation (Puddu et al., 2008; Pfander and Diffley, 2011). Notably, Rad53 signaling contributes to inhibit DNA end resection by inhibiting the action of the Exo1 nuclease (Morin et al., 2008; Segurado and Diffley, 2008) and potentially promoting Rad9 retention at the DNA lesion (Gobbini et al., 2015). Therefore, the Mec1-dependent shift in Dpb11 interaction from Rad9 to Slx4 is a key event in this circuitry, resulting in a drastically different output in resection control. It is tempting to speculate that early in the response to DNA lesions, the Dpb11–Rad9

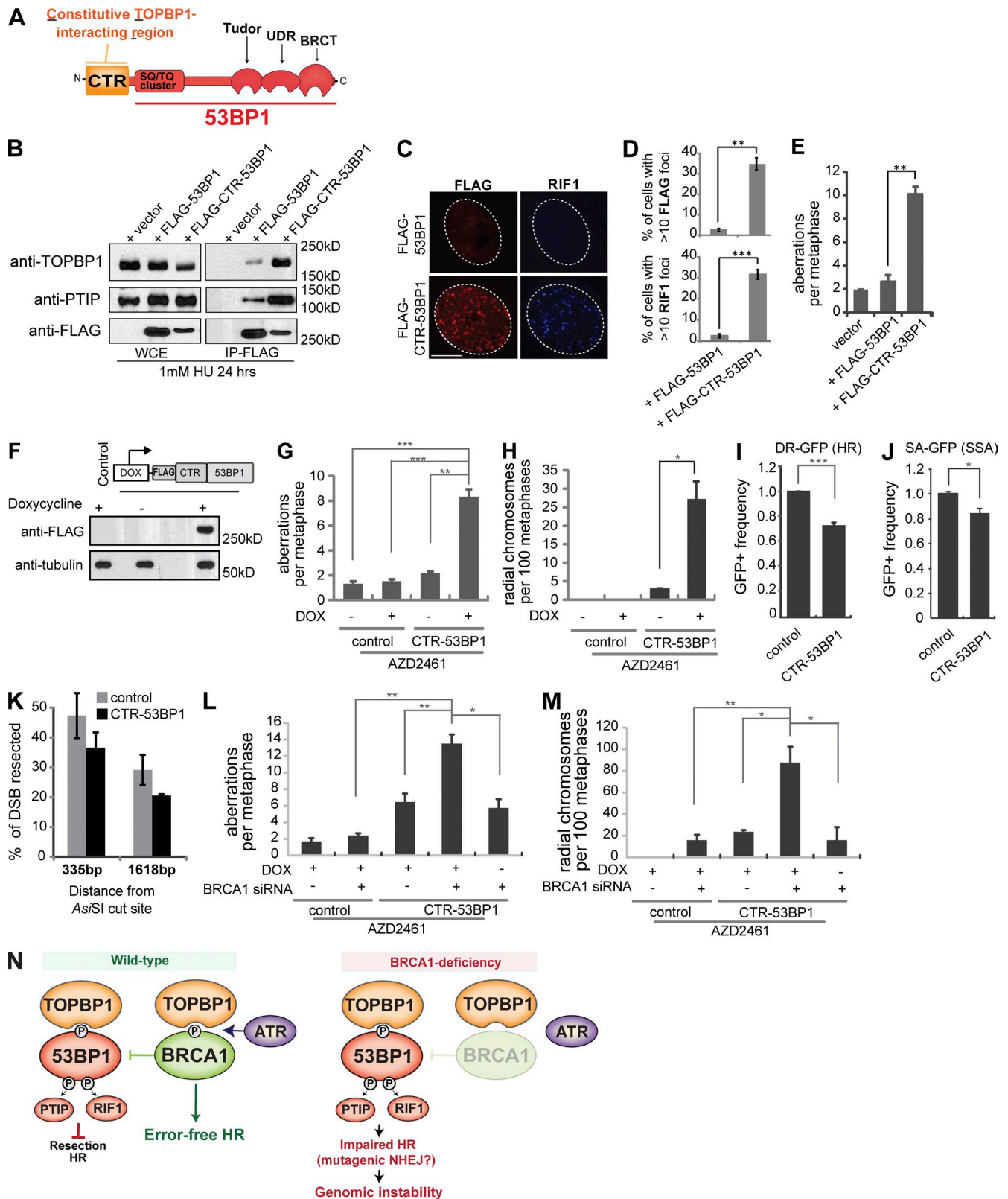


Figure 5. Hyperstabilization of the TOPBP1–53BP1 interaction promotes 53BP1 recruitment and impairs HR-mediated repair. (A) Schematic illustration of the CTR-53BP1 chimera in which a 120–amino acid fragment in the N-terminal domain of RFC1 was fused to full-length 53BP1. (B) Coimmunoprecipitation experiment pulling down CTR-53BP1 and probing for TOPBP1 and PTIP in HEK293T cells treated with 1 mM HU for 24 h. Ectopic 53BP1 and CTR-53BP1 containing an N-terminal FLAG-tag were transiently overexpressed. WCE, whole cell extract. (C) Immunofluorescence of U2OS cells transfected with FLAG-53BP1 or FLAG-CTR-53BP1 and treated with 1 mM HU for 24 h followed by a 3-h release in fresh media. In our experience, this short release period enhanced the visualization of replication stress–induced nuclear foci for the indicated proteins. White dotted lines indicate nuclear boundaries. Displayed images were extracted from the panels in Fig. S2 A and show bars and DAPI staining. Bar, 10 μ m. (D) Quantitation of results from the experiment shown

complex activates the checkpoint to promote, among other outputs, a protection for replication forks and DSB ends from detrimental and unregulated resection. With the subsequent buildup in Mec1 signaling at these sites, coordinated HR-mediated repair is evoked by the phosphorylation of Slx4, which promotes the Dpb11–Slx4 interaction, destabilizes Rad9 engagement at DNA lesions, and therefore favors resection. Consistent with this model, our results using fusion proteins recapitulate the importance of Dpb11 for the stabilization of Rad9 at DNA lesions and show that an MBD module competing for binding to the 9-1-1 complex and γ -H2A can completely counteract the engagement of Rad9 and strongly promote resection.

In human cells, we propose that, similar to the Dpb11-mediated circuitry, TOPBP1 also mediates a phosphoregulated circuitry for HR control. Our results are consistent with a model in which the BRCA1–TOPBP1 interaction plays a role analogous to the Dpb11–Slx4 interaction in yeast to prevent TOPBP1-mediated stabilization of 53BP1 at DNA lesions. Interestingly, the mammalian circuitry seems to follow a similar regulatory logic we observed in the yeast system. Although TOPBP1 interacts with both BRCA1 and 53BP1, the ATR kinase specifically promotes the TOPBP1–BRCA1 interaction but not the TOPBP1–53BP1 interaction. We speculate that the ATR-mediated TOPBP1–BRCA1 interaction functions similarly to the Dpb11–Slx4 interaction, counteracting the TOPBP1–53BP1 interaction and destabilizing the engagement of 53BP1 at DNA lesions. We note that human SLX4 was also identified as a TOPBP1 interactor, consistent with a previous study (Gritenaite et al., 2014). However, the interaction of TOPBP1 with SLX4 is not enhanced by replication stress, suggesting a fundamentally distinct mode of interaction compared with the Dpb11–Slx4 interaction in yeast.

Much remains unclear about the mechanism and regulation of TOPBP1 interactions with BRCA1 and 53BP1. Dissecting the mechanism of these interactions will be essential to better understand how TOPBP1 and ATR control resection and how TOPBP1 helps promote 53BP1-mediated repair. Regulation of the TOPBP1–BRCA1 seems more complex than regulation of the Dpb11–Slx4 interaction in yeast, as it has been previously shown that ATM and DNA-PK can also promote the TOPBP1–BRCA1 interaction (Greenberg et al., 2006). Because those experiments were performed in response to ionizing radiation,

further work is necessary to precisely define the role of each kinase under distinct forms of DNA damage. Nonetheless, our results support that ATR plays a more prominent role during replication stress in mediating the TOPBP1–BRCA1 interaction as compared with ATM and DNA-PK. This is congruent with the idea that ATR is a key inducer of HR-mediated repair during replication stress. Generation of separation-of-function *BRCA1* mutants bearing mutations in phosphorylation sites that mediate interaction with TOPBP1 will be required to further determine the precise extent to which ATR-mediated HR depends on the TOPBP1–BRCA1 interaction. We envision that ATR-dependent formation of the TOPBP1–BRCA1 interaction is likely one of the key events required for ATR-mediated resection. As such, understanding the TOPBP1-mediated circuitry for the phosphoregulation of resection could have implications for understanding how to best use ATR inhibitors in cancer therapy.

It has been recently reported that depletion of TOPBP1 abrogates RAD51 loading to chromatin and formation of RAD51 foci but does not impair DNA end resection or RPA loading (Moudry et al., 2016). Based on our model, we predict that in the experimental setup of Moudry et al. (2016), the absence of TOPBP1 would also impair 53BP1-mediated resection block, thereby allowing productive DNA end processing to occur. In fact, the scenario would be similar to what is observed in cells lacking both BRCA1 and 53BP1, where resection is restored as compared with cells lacking only BRCA1 (Bunting et al., 2010). Therefore, the findings by Moudry et al. (2016) are fully consistent with our model that TOPBP1 is important to promote 53BP1 functions in DNA repair. Consistent with this model, stabilization of the TOPBP1–53BP1 interaction reduced the efficiency of HR-mediated repair and resection. We acknowledge that our method for monitoring resection is not yet set to measure resection of distances farther from the break and that the effect of blocking long-range resection at distances >2 kb from the break may be stronger, as we observed for yeast. The mild effect in resection may also be related to the expression level of the CTR-53BP1 fusion, which was not dramatically higher than the expression level of endogenous 53BP1 (Fig. S3 B). In the future, it will be interesting to measure resection in mutants where the TOPBP1–53BP1 interaction is disrupted and determine whether these mutants may restore HR-mediated repair in BRCA1-deficient cells. Along these lines, it will be

in C scoring FLAG and RIF1 foci in transfection-positive cells. Graphs represent results from at least three independent experiments, and >150 transfected cells were scored per replicate. (E) Analysis of chromosomal abnormalities in metaphases of HEK293T cells treated with 1 μ M ATR inhibitor (VE-821) and 3 μ M PARP inhibitor (AZD2461). Metaphase spreads were prepared as described in the Metaphase spread preparation section of Materials and methods. $n > 45$ metaphases were analyzed in each replicate. (F) Immunoblot showing the DOX-induced expression of CTR-53BP1. CTR-53BP1 is stably integrated in HEK293 cells using a Flp-In T-REx system. (G and H) Analysis of metaphase chromosomal abnormalities in HEK293 cells expressing CTR-53BP1 in response to PARP inhibitor. Cells were treated with DOX for 48 h, and 3 μ M AZD2461 was added for another 24 h. Cells were then analyzed for chromosomal aberrations. The total number of chromosomal aberrations (breaks, fusions, acentrics, and radials; G) and a subset of radial chromosomes (H) were scored. $n > 30$ metaphases were analyzed in each replicate, and each condition was repeated at least three times. (I) HR efficiency was measured in CTR-53BP1-expressing cells using the DR-GFP reporter system. HEK293 cells with CTR-53BP1 stably integrated were treated with DOX and transfected with both the pDR-GFP and pCBASceI plasmids. The GFP-positive (GFP+) cell population was analyzed by flow cytometry 48 h after transfection, and the percentages of GFP-positive cells were calculated in each condition. The data are normalized to the control cell line stably integrated with an empty vector. (J) Efficiency of SSA-mediated repair was measured in cells transiently expressing CTR-53BP1 or empty vector. U2OS SA-GFP cells were cotransfected with plasmids expressing CTR-53BP1 and I-SceI. GFP-positive cells were then analyzed 72 h after transfection as described in I. (K) Measurement of DSB resection in cells expressing CTR-53BP1 by qPCR. HEK293 cells with both CTR-53BP1 and AsiSI-ER stably integrated were treated with DOX for 48 h to induce CTR-53BP1 expression, followed by 4OHT treatment for another 6 h to induce DSB. (L and M) Analysis of metaphase chromosomal abnormalities in HEK293 cells with DOX-inducible CTR-53BP1 upon depletion of BRCA1. HEK293 cells with CTR-53BP1 stably integrated were transfected with BRCA1 siRNA or control siRNA. At 48 h after transfection, cells were treated with 3 μ M AZD2461 for 24 h and then harvested. The total numbers of chromosomal aberrations (L) and radial chromosomes (M) were scored. BRCA1 knockdown efficiency is shown in Fig. S5 B. (N) Model for the role of TOPBP1 in mediating a phosphorylation-regulated circuitry for the control of recombinational DNA repair. See Discussion for details. P, phosphorylation. All graphs displayed in this figure are plotted using means \pm SEM from at least three independent experiments. P-values were determined based on a two-tailed Student's *t* test. *, $P < 0.05$; **, $P < 0.01$; ***, $P < 0.001$.

important to define how 53BP1 (and the TOPBP1–53BP1 interaction) promotes chromosomal abnormalities upon BRCA1 deficiency. Although these abnormalities have been proposed to be driven by 53BP1-mediated NHEJ, it is conceivable that genomic instability may arise through deregulated and error-prone HR-mediated repair, as the action of 53BP1 in negatively regulating resection may not completely block resection but instead result in aberrantly regulated resection. Overall, our findings presented here provide important insights into the mode of action of TOPBP1^{Dpb11} in the control of DNA repair and should have implications for understanding how genomic instabilities and cancer arise in individuals with defective HR machineries.

Materials and methods

Yeast strains, plasmids, media, and growth conditions

Strains generated in this study were derived from S288C or JKM139. HA and FLAG tags were inserted by HR at specific genomic loci (all proteins were tagged at the C terminus, and the expression was verified by Western blotting). Tagged strains were assayed for sensitivity to MMS to ensure that they displayed similar sensitivity as wild-type strains. Standard cloning methods were used to generate the plasmids for this study. The *BRCT3/4-RAD9* chimera was generated using a stitch PCR protocol. In brief, we fused the *RAD9* promoter (450 bp upstream of the start codon) to the *BRCT3/4* of *DPB11* (corresponding to amino acids 292–600 of Dpb11), and the resulting PCR product was stitched to the *RAD9-3×FLAG* sequence (see Fig. 1 B for the schematic illustration of the resulting chimeric protein). The final PCR product was subsequently cloned into *pRS416* (for ectopic expression) or *pFA6A* (for integration at the endogenous *RAD9* locus). All point mutations were generated by site-directed mutagenesis using the PrimeSTAR Max DNA Polymerase (Takara Bio Inc.). The plasmid for expression of the MBD fusion protein was constructed as previously described (Cussiol et al., 2015). All yeast strains and plasmids used in this study are described in Tables S1 and S2, respectively. Yeast cells expressing genes with the indicated epitope tags were cultured in YPD (yeast-peptone-dextrose) medium or in synthetic complete medium lacking uracil and/or tryptophan when carrying an expression plasmid with *URA3* or *TRP1* (derivatives from *pRS416* and *pRS414*, respectively). Cells were grown to the log phase, subjected to MMS treatment as specified in the figures, and collected by centrifugation. For the experiments using the JKM139 and YMV80 strains, cells were grown in YP (yeast-peptone) medium enriched with 2% glucose (YPD), 3% raffinose (YP raff), or 3% raffinose and 2% galactose (YP raff gal). All synchronization experiments were performed at 28°C.

ChIP analysis in yeast

For ChIP analysis, exponentially growing JKM139-derivative strains were nocodazole arrested. After HO induction, samples were collected at the indicated time points and cross-linked with formaldehyde for 10 min. After centrifugation, cell pellets were washed in HBS buffer (50 mM Hepes, pH 7.5, 140 mM NaCl, and 1 mM EDTA, pH 8) and then lysed in lysis buffer (50 mM Hepes, pH 7.5, 140 mM NaCl, 1 mM EDTA, pH 8, and 1% Triton X-100) by bead beating. After centrifugation for 30 min at 4°C, the chromatin pellet was resuspended in lysis buffer supplemented with Complete EDTA-free protease inhibitor cocktail (Roche) and 1 mM PMSF and was subjected to sonication. After two steps of centrifugation, soluble sheared chromatin was incubated with anti-FLAG agarose beads (Sigma-Aldrich) for 2 h at 4°C. After immunoprecipitation, beads were washed with the following buffers: HBS, HiSalt (50 mM Hepes, pH 7.5, 1 M NaCl, and 1 mM

EDTA, pH 8), TL (20 mM Tris-HCl, pH 7.5, 250 mM LiCl, 1 mM EDTA, pH 8, and 0.5% Triton X-100), TE (20 mM Tris-HCl, pH 7.5, and 1 mM EDTA, pH 8). Beads were resuspended with TE + 1% SDS and incubated at 65°C for 2 min, and protein-bound chromatin was separated using a magnetic support. Reverse cross-linking was done overnight at 65°C, and DNA was purified using spin columns (Promega). Immunoprecipitated DNA and the corresponding input sample were analyzed by a real-time qPCR using a CFX connect (Bio-Rad Laboratories). The oligonucleotides used are listed in Table S6. Data are presented as fold enrichment at the HO cut site (0.15 kb from the DSB) over that at the *PRE1* locus on chromosome V and then normalized by the corresponding input sample. The final fold enrichment value was then normalized on the fold enrichment of the t_0 sample.

Coimmunoprecipitation procedure in yeast

Coimmunoprecipitation experiments for yeast lysates were performed as described previously (Cussiol et al., 2015). In brief, cells with the indicated epitope tags were grown until the log phase in YPD and treated with MMS or arrested with nocodazole followed by phleomycin treatment (concentration and incubation time used for each experiment are described in the figure legends). After centrifugation, pellets were washed with TE + PMSF and kept at –80°C before cell lysis. Approximately 0.1 g of cell pellet of each strain was lysed by bead beating at 4°C in 1 ml of lysis buffer (50 mM Tris-HCl, pH 7.5, 0.2% Tergitol, 150 mM NaCl, 5 mM EDTA, Complete EDTA-free protease inhibitor cocktail, 5 mM sodium fluoride, and 10 mM β-glycerolphosphate). Samples were normalized by protein concentration. For Dpb11-Rad9 coimmunoprecipitation, cell lysates were precleared by incubating with 100 μl of human IgG Sepharose beads (IgG Sepharose 6 Fast Flow; 17-0969-01; GE Healthcare) for 30 min at 4°C. Precleared whole-cell lysates were then incubated with anti-FLAG agarose resin (Sigma-Aldrich) for 2 h at 4°C. After three washes with lysis buffer, bound proteins were eluted for 10 min at room temperature with 0.5 μg/ml FLAG peptide (Sigma-Aldrich) in 100 mM Tris-HCl and 0.2% Tergitol.

Mammalian expression plasmids

BRCA1, 53BP1, and CTR-53BP1 expression vectors were first generated in the corresponding gateway-compatible entry clones in pDONR223 (Thermo Fisher Scientific). 53BP1 and BRCA1 were amplified from pcDNA5-FRT/TO-eGFP-53BP1 (Addgene plasmid 60813; a gift from D. Durocher; Fradet-Turcotte et al., 2013) and pCR3-BRCA1 (a gift from R. Weiss, Cornell University, Ithaca, NY). The CTR-53BP1 fragment was created using overlapping PCR to fuse the PCR product of CTR (1–120-aa of RFC1) with that of full-length 53BP1. CTR-53BP1, BRCA1, and 53BP1 were then each cloned into the pHAGE-CMV-FLAG-HA-puro gateway destination vector, provided by A. Smogorzewska (The Rockefeller University, New York, NY). To generate CTR-53BP1 vectors bearing mutations in the UDR and tudor domains of 53BP1, we used the QuikChange Multi Site-Directed Mutagenesis kit (200515; Agilent Technologies) to mutate the entry clone, and the mutated entry clones were then transferred to the destination vector. For TOPBP1 cloning, TOPBP1 cDNA was amplified from pGEX6P1-TOPBP1 (Addgene plasmid 20375; a gift from A. Sancar; Choi et al., 2009) and then cloned into pcDNA3-3HA through EcoRI and NotI restriction digestion. TOPBP1 mutants bearing mutations in BRCT1, BRCT5, and BRCT7 were created using the QuikChange Multi Site-Directed Mutagenesis kit. FLAG-HA-CTR-53BP1 was amplified from the previously cloned gateway expression vector pHAGE-CMV-FLAG-HA-CTR-53BP1-puro and inserted into pcDNA5-FRT/TO vector using the Gibson Assembly Cloning kit (E5510S; New England Biolabs, Inc.). This vector was then used for the generation of stable cell lines with the DOX-inducible expression of CTR-53BP1.

Mammalian cell culture

Human U2OS, HEK293T, and HEK293 Flp-In T-REx cell lines were grown in DMEM supplemented with 10% bovine calf serum, non-essential amino acid, and penicillin/streptomycin (Corning). The HEK293 Flp-In T-REx cell line for the expression of DOX-inducible FLAG-CTR-53BP1 and a control cell line with empty vector integrated were generated by stable transfection using the Flp-In T-REx system (R78007; Thermo Fisher Scientific) according to the manufacturer's instructions and were cultured in 10% bovine calf serum/DMEM supplemented with 50 µg/ml hygromycin B. To induce protein expression in HEK293 Flp-In T-REx cell lines, 2 µg/ml DOX was added to the culture media for 48 h. Plasmid transfections were performed using homemade polyethylenimine (Polysciences, Inc.), jetPRIME polyethylenimine (Polyplus), or Lipofectamine 2000 (Thermo Fisher Scientific). The siRNA transfections were performed using Lipofectamine RNAiMax (Thermo Fisher Scientific). At 48 h after transfection, cells were subjected to the indicated drug treatments and then fixed or harvested for microscopy and immunoprecipitation experiments. Specifically for immunoprecipitation experiments, HEK293T cells were treated for either 24 h with 1 mM HU or 14 h with 100 ng/ml nocodazole before harvesting. For the ATR inhibition experiments (Fig. 4 E), cells were pretreated with the indicated inhibitors, 10 µM ATR inhibitor (VE-821), 10 µM ATM inhibitor (KU-55933), and 5 µM DNA-PK inhibitor (NU7441), for 45 min before additional treatment with 2.5 mM HU for 30 min.

Coimmunoprecipitation procedures in mammalian cells

For coimmunoprecipitation experiments, cell pellets were lysed for 30 min on ice in modified radioimmunoprecipitation assay (RIPA) buffer (50 mM Tris-HCl, pH 7.5, 150 mM NaCl, 1% tertigol, 0.25% sodium deoxycholate, and 5 mM EDTA) supplemented with Complete EDTA-free protease inhibitor cocktail, 5 mM sodium fluoride, 10 mM β-glycerolphosphate, 1 mM PMSF, and 0.4 mM sodium orthovanadate. Protein lysates were cleared by 10-min centrifugation to pellet cell debris and then were incubated with anti-TOPBP1 resin, anti-HA, or FLAG agarose beads (Sigma-Aldrich) for 4 h at 4°C. Immunoprecipitates were then washed three times with the modified RIPA buffer and then eluted using three resin volumes of the elution buffer (0.5 µg/ml FLAG peptide in 50 mM Tris-HCl and 0.2% tertigol for anti-FLAG resin; 100 mM Tris-HCl, pH 8.0, and 1% SDS for others).

Immunoblotting analysis

Whole-cell lysates and eluents were denatured with 3× SDS sample buffer (composed of bromophenol blue, stacking gel buffer, 50% glycerol, 3% SDS, and 60 mM DTT) and resolved on SDS-PAGE gels. Proteins were then transferred onto polyvinylidene fluoride membranes and probed with the desired antibodies.

Mass spectrometry analysis

For mammalian stable isotope labeling with amino acids in cell culture (SILAC) experiments, HEK293T cells were grown in SILAC DMEM media lacking arginine and lysine (88425; Thermo Fisher Scientific) supplemented with 10% dialyzed FBS and penicillin/streptomycin. "Light" DMEM was supplemented with "light" (normal) arginine and lysine; "heavy" DMEM was supplemented with "heavy" lysine (¹³C₆, ¹⁵N₂) and "heavy" arginine (¹³C₆, ¹⁵N₄). Cells were treated with 1 mM HU for 24 h or with 100 ng/ml nocodazole for 14 h before harvesting. TOPBP1 was immunoprecipitated using affinity-purified anti-TOPBP1 antibodies or antibodies that recognize the according epitope tags. Immunoprecipitated proteins were then reduced, alkylated, precipitated, and digested by trypsin. The peptides were desalted, dried, reconstituted in 80% acetonitrile and 1% formic acid, and then fractionated by

hydrophilic interaction chromatography. Fractions were dried, reconstituted in 0.1% trifluoroacetic acid, and analyzed by liquid chromatography–tandem mass spectrometry using a mass spectrometer (Q Exactive Orbitrap; Thermo Fisher Scientific). The capillary column was 20 cm long with a 125-µm inner diameter, packed in-house with 3-µm, 200-Å C18AQ particles (Prontosil). Peptides were separated over an 80-min linear gradient of six to 40% acetonitrile in 0.1% formic acid at a flow rate of 200 nL/min (Bastos de Oliveira et al., 2015). Xcalibur 2.2 software (Thermo Fisher Scientific) was used for the data acquisition, and the Q Exactive was operated in the data-dependent mode. Survey scans were acquired in the Orbitrap mass analyzer over the range of 380 to 2,000 m/z with a mass resolution of 70,000 (at m/z 200). The maximum ion injection time for the survey scan was 80 ms with a 3e6 automatic gain-control target ion. Tandem mass spectrometry spectra was performed by selecting up to the 10 most abundant ions with a charge state of 2, 3, or 4 and with an isolation window of 2.0 m/z. Selected ions were fragmented by higher energy collisional dissociation with a normalized collision energy of 27, and the tandem mass spectra was acquired in the Orbitrap mass analyzer with a mass resolution of 17,500 (at m/z 200). For the database search, raw tandem mass spectrometry spectra were searched in a SORCERER system (Sage-N Research, Inc.) using SEQUEST software (Thermo Fisher Scientific), and all entries were from the human UniProt proteome database. The following parameters were used in the database search: semitryptic requirement, a mass accuracy of 15 ppm for the precursor ions, a differential modification of 8.0142 D for lysine and 10.00827 D for arginine, and a static mass modification of 57.021465 D for alkylated cysteine residues. The XPRESS software, part of the Trans-Proteomic Pipeline (Seattle Proteome Center), was used to quantify all the identified peptides (Bastos de Oliveira et al., 2015).

Chemicals and antibodies

PARP inhibitor (AZD2461), ATM inhibitor (KU-55933), DNA-PK inhibitor (NU7441), and ATR inhibitor (VE-821) were purchased from Selleckchem. Nocodazole was purchased from EMD Millipore. HU and MMS were purchased from Acros Organics. Antibodies used for the detection of yeast proteins were all mouse antibodies: anti-Rad53 antibody (clone Mab EL7; 1:30 dilution; Abcam); anti-FLAG (M2 F1804; 1:5,000 dilution; Sigma-Aldrich), and anti-HA (12CA5; 1:10,000 dilution; Roche). The following antibodies were used for the detection of proteins in human cells: mouse antibodies include anti-FLAG (M2; F1804; Sigma-Aldrich), anti-HA.11 (MMS-101P; Covance), anti-phosphohistone H2A.X (pSer139; 05-636; JBW301; EMD Millipore), anti-RPA (ab2175; Abcam), and anti-BRCA1 (OP92; MS110; EMD Millipore); rabbit antibodies include anti-FLAG (PA1-984B; Thermo Fisher Scientific), anti-53BP1 (NB100-304; Novus Biologicals), anti-phospho-KAP-1 (S824; A300-767A-T; Bethyl), anti-RAD51 (PC130; EMD Millipore), and anti-phospho-CHK1 (pSer345; 2341; Cell Signaling Technology). Goat antibody was used for detection of RIF1 (sc-55979; Santa Cruz Biotechnology, Inc.). The anti-TOPBP1 and anti-BRCA1 antibodies, provided by R. Freire (Hospital Universitario de Canarias, Tenerife, Spain), were raised in rabbits injected with amino acids 900–1200 of human TOPBP1 and amino acids 1350–1650 of human BRCA1, respectively (Danielsen et al., 2009; Kakarougkas et al., 2013). The anti-PTIP antibody, provided by K. Ge, was generated against amino acids 274–472 of mouse PTIP by immunizing rabbits (Cho et al., 2009).

RNAi

Cells were transfected with the indicated siRNA using Lipofectamine RNAiMAX according to the manufacturer's instructions. The siRNA against BRCA1 (BRCA1 HSS101089; 5'-AAAUGUCACUCUGAG

AGGAUAGCCC-3') was purchased from Thermo Fisher Scientific. Medium GC stealth RNAi siRNA Negative Control (12935300; Thermo Fisher Scientific) was used as control.

Immunofluorescence

U2OS cells grown on glass coverslips were fixed with 3.7% formaldehyde/PBS for 15 min at room temperature. Cells were then permeabilized with 0.2% Triton X-100 in PBS for 5 min at room temperature, blocked with 5% BSA for 30 min at 37°C, and then incubated with primary antibodies for 1 h at room temperature. This was followed by three washes with PBS and secondary antibody incubation with Alexa Fluor 488 donkey anti-rabbit (A-21206), Alexa Fluor 594 donkey anti-mouse (A-21203), or Alexa Fluor 647 donkey anti-goat (A-21447; Thermo Fisher Scientific). Next, cells were washed with PBS three times and mounted using Vectashield Antifade mounting medium with DAPI (H1200; Vector Laboratories).

Microscopy analysis

Images were acquired at room temperature using a spinning-disc confocal microscope (CSU-X; Yokogawa Electric Corporation and Intelligent Imaging Innovations) on an inverted microscope (DMI600B; Leica Biosystems) with a 63 \times , 1.4 NA objective lens for mammalian cells or a 100 \times , 1.46 NA objective lens for yeast and mammalian cells and a charge-coupled device camera (cool-SNAP HQ2; Photometrics) for mammalian cells or an electron-multiplying charge-coupled device camera (QuantEM; Photometrics) for yeast cells. 488, 561, and 640-nm laser lines were used for the excitation of Alexa Fluor 488-, 594-, and 647 dyes, respectively, in immunofluorescence microscopy. 488- and 561-nm laser lines were used for the detection of mRuby and GFP-tagged proteins in yeast cells, respectively. SlideBook software (Intelligent Imaging Innovations) was used to obtain Z stack images. Maximum intensity projections were created in the Slidebook software for foci number analysis. For the analysis of foci formation of mammalian RIF1 or of FLAG-tagged 53BP1 or CTR-53BP1, >150 transfected cells for each condition were imaged and analyzed per replicate. Cells with >10 distinct RIF1 or FLAG foci were scored as foci-positive cells. The percentages of RIF1 or FLAG foci-positive cells were calculated based on the arithmetic mean and SEM derived from three biological replicates. A two-tailed Student's *t* test with 95% confidence interval was used to determine whether the difference between the means of two sets of values was significant. For yeast Rfa1 and Rad52 foci analysis, cells were grown in synthetic complete lacking tryptophan media until the log phase (OD = 0.3), and MMS (0.033%) was added to the cells for 2 h at 30°C. Next, cells were washed in sterile water and resuspended in fresh synthetic complete media. Live yeast cultures were mounted on an agarose slide pad (1.2% agarose in SC-TRP media) and >150 cells were scored for each replicate. The percentages of cells with multiple Rad52-mRuby2 foci or containing a single Rfa1-mRuby2 focus or multiple Rfa1-mRuby2 foci were calculated based on the arithmetic mean and SEM derived from three independent replicates. A two-tailed Student's *t* test with a 95% confidence interval was used to determine whether the difference between the means of two sets of values was significant.

Metaphase spread preparation

HEK293T cells were cotransfected with plasmids for expression of 53BP1 or CTR-53BP1, together with a plasmid for expression of H2B-GFP (Addgene plasmid 11680) used as a marker for transfection. In Flp-In T-REx 293 cells with CTR-53BP1 stably integrated, protein expression was induced using 2 μ g/ml DOX for 48 h, followed by the indicated genotoxin treatment. Cells were then treated

with 150 ng/ml colcemid for 1 h and collected by trypsinization followed by centrifugation. Cell pellets were resuspended in hypotonic buffer (0.034 M KCl) for 6 min at 37°C and then fixed in fixation buffer (3:1 of methanol and acetic acid) overnight. Fixed cells were then washed with fixation buffer three times, spotted onto a microscope slide, and mounted using Vectashield Antifade mounting medium with DAPI. Metaphase spreads were imaged using the CSU-X spinning disc confocal microscope with 100 \times , 1.46 NA objective. Chromosomal aberrations were then scored. Each condition was repeated at least two times independently, and 30–50 metaphases were analyzed per replicate. The two-tailed Student's *t* test was used for statistical analysis.

Cell survival assay

HEK293 Flp-In T-REx cells with stably integrated CTR-53BP1 and the control cell line were seeded in DOX-containing media for 48 h to induce CTR-53BP1 expression. Cells were then subjected to genotoxin treatment in the continuous presence of DOX for 72 h before cells were counted. The percentage of survival was calculated, and the graph was plotted based on at least three independent experiments showing means \pm SEM. The two-tailed Student's *t* test was used for statistical analysis.

Measurement of resection at HO-induced DSB in yeast

HO-induced DSB resection was measured in JKM139 background by qPCR analysis as described previously (Ferrari et al., 2015). Cells were arrested in G2/M by nocodazole treatment before HO induction. Genomic DNA was extracted and digested or mock treated with RsaI restriction enzyme (New England Biolabs, Inc.), which cuts inside the amplicons at 0.15, 1.4, and 4.8 kb from the HO cut site, but not in the *PRE1* control region on chromosome V. PCR values are then normalized by the cut efficiency calculated by Southern blot analysis, with a probe around the HO cut site.

SSA repair analysis in yeast

SSA repair efficiency of an HO endonuclease-induced DSB in YMV80 background was analyzed using Southern blotting procedures (Vaze et al., 2002; Ferrari et al., 2015). In brief, cells grown in YP medium containing 3% lactate at 28°C reaching a density of 5×10^6 cells/ml were arrested with 20 μ g/ml nocodazole, followed by the addition of 2% galactose to trigger a single DSB by inducing HO endonuclease expression. Cells remained arrested after DSB induction as confirmed by FACS and monitoring nuclear division. At the indicated time points, cells were collected to isolate genomic DNA, which was then subjected to Southern blotting analysis to determine the loss of 5' ends at the HO cut *MAT* locus (Lee et al., 1998; Vaze et al., 2002; Clerici et al., 2005). Each experiment was repeated at least three times independently, and one representative result is shown.

DR-GFP assay

HEK293 Flp-In T-REx cells with CTR-53BP1 or empty vector stably integrated were cultured in DMEM containing 2 μ g/ml DOX and transfected with plasmid-carrying DR-GFP (pDR-GFP; Addgene plasmid 26475) and pCBASceI (Addgene plasmid 26477; gifts from M. Jasini; Pierce et al., 1999). In the case of BRCA1 knockdown, cells were transfected with BRCA1 siRNA (BRCA1 HSS101089; Thermo Fisher Scientific), and 48 h after siRNA transfection, cells were transfected with the plasmids pDR-GFP and pCBASceI. The GFP-positive cell population was analyzed 48 h after transfection. The percentage of GFP-positive cells was quantified in each condition by flow cytometry analysis using FACS Aria Fusion (BD) and normalized by the control cell line where empty vector was integrated. The data are presented as means \pm SEM ($n > 3$).

SSA repair assay in mammalian cells

U2OS-SA-GFP cells (a gift from J. Stark; Gunn and Stark, 2012) were cotransfected with 0.5 μ g I-SceI plasmid and 0.5 μ g of plasmid expressing CTR-53BP1 or empty vector using Amaxa Nucleofector II in a 60-mm plate. Cells were grown for 3 d, harvested, and subjected to flow cytometry analysis using FACSAria and FACSDiva software (BD) to determine the percentage of GFP-positive cells.

Measurement of resection at one AsiSI-induced DSB in human cells

Resection assay was performed as described previously by Zhou et al. (2014) with some modifications. In brief, HEK293 cells stably expressing CTR-53BP1 or control cells stably transfected with an empty vector were transfected with the pBabe-AsiSI-ER plasmid (Iacovoni et al., 2010) using Lipofectamine 3000 (Thermo Fisher Scientific), and selection was performed using 1 μ g/ml puromycin. Cells were seeded on a well of a 6-well plate. After 24 h, 2 μ g/ml DOX was added to induce expression of the CTR-53BP1 protein. 48 h after induction, 300 nM 4-hydroxytoremoxifen (4OHT; Sigma-Aldrich) was added for 6 h to create AsiSI-induced DSBs. For experiments with transient expression of CTR-53BP1, U2OS-AsiSI-ER cells were transfected with empty vector or the plasmid-expressing CTR-53BP1 using Amaxa Nucleofector II. 4OHT was added for 6 h to induce DSBs 48 h after transfection. After 4OHT treatment, cells were collected, and genomic DNA was extracted and eluted in a final volume of 100 μ l using the NucleoSpin Tissue kit (MACHEREY-NAGEL). Then, 15 μ l genomic DNA was digested or mock digested with 20 U BsrGI enzyme (New England Biolabs, Inc.) in a final volume of 90 μ l at 37°C overnight. The mix was incubated at 80°C for 20 min to inactivate the BsrGI enzyme and diluted twofold. 5 μ l of diluted mix from either the digested or mock-digested sample (~40 ng) was used as a template in a 25- μ l qPCR reaction containing 12.5 μ l of 2 \times master mix containing SYBR green (Genespin) and 0.2 μ M of each primer using a CFX Connect Real Time system (Bio-Rad Laboratories). Primers listed in Table S7 were used to analyze resection at 335 and 1,618 bp from the AsiSI cut site on Chromosome 1. The percentage of resection at selected DSB sites was determined from qPCR reactions by using the formula, % DSB resected = $100 / [(1 + 2^{\Delta Ct}) / 2] / f$ (Zierhut and Diffley, 2008), where ΔCt is obtained by subtracting the Ct values of mock-digested samples from the Ct values of digested samples, and f is the cut efficiency calculated from qPCR reaction with the primers “Across DSB” using the formula, $f = 1 - 2^{-\Delta Ct}$, where ΔCt is obtained by subtracting the Ct value of the untreated sample from the Ct value of the 4OHT-treated sample.

Online supplemental material

Fig. S1 shows that BRCA1 and 53BP1 are not detected in pull-downs of 53BP1 and BRCA1, respectively, and that their interaction with TOPBP1 is oppositely regulated by HU. Fig. S2 demonstrates that CTR-53BP1 promotes the recruitment of the NHEJ factor RIF1 to DNA damage foci. Fig. S3 presents the characterization of a HEK293 stable cell line generated for the DOX-inducible expression of CTR-53BP1. Fig. S4 shows that the expression of CTR-53BP1 leads to a stronger impairment in HR compared with overexpression of 53BP1. Fig. S5 shows the data used for determining the effect of CTR-53BP1 expression and BRCA1 depletion on the accumulation of chromosomal aberrations. Tables S1 and S2 describe the yeast strains and plasmids used in this study, respectively. Tables S3 and S4 show the mass spectrometry analysis results of TOPBP1 interactions in cells arrested by HU and nocodazole, respectively. Table S5 shows the mass spectrometry analysis result comparing TOPBP1 interactions in HU versus nocodazole. Table S6 lists the oligonucleotide sequences used for CHIP and DSB resection analysis in yeast. Table S7 lists the oligonucleotide sequences used for the measurement of DSB resection in human cell lines.

Acknowledgments

We thank the members of all laboratories involved for comments and suggestions.

This work was supported by grants from the National Institutes of Health to M.B. Smolka (R01-GM097272) and to R.S. Weiss (R01-CA108773), to A. Pellicoli from the Associazione Italiana per la Ricerca sul Cancro (AIRC IG-15488) and Fondazione Cariplo, and to R. Freire from the Spanish Ministry of Economy and Competitiveness (SAF2013-49149-R and BFU2014-51672-REDC) and Fundación CajaCanarias (AP2015/008). J.R. Sims was supported by a National Institutes of Health training grant (T32GM007273).

The authors declare no competing financial interests.

Author contributions: M.B. Smolka conceived the project. M.B. Smolka, Y. Liu, J.R. Cussiol, A. Pellicoli, and D. Dibitetto designed the experiments. Y. Liu performed mass spectrometry, coimmunoprecipitation, immunofluorescence microscopy, genotoxin sensitivity assays, and HR measurement experiments in mammalian cells. J.R. Cussiol generated the BRCT3/4-Rad9 and MBD chimeras and performed genotoxin sensitivity assays and Rad53 activation analysis in yeast. J.R. Cussiol and Y. Liu performed microscopy experiments in yeast. D. Dibitetto performed ChIP experiments, SSA assays, and resection analysis in yeast. M.B. Smolka performed coimmunoprecipitation experiments in yeast and analyzed mass spectrometry data in mammalian cells. Y. Liu and J.R. Sims performed metaphase spread analysis. R. Freire generated anti-TOPBP1 and anti-BRCA1 antibodies. S. Twayana and F. Marini did the resection and SSA assays in mammalian cells. M.B. Smolka, Y. Liu, and J.R. Cussiol wrote the manuscript. M.B. Smolka, Y. Liu, J.R. Cussiol, D. Dibitetto, J.R. Sims, R.S. Weiss, R. Freire, F. Marini, and A. Pellicoli edited and reviewed the manuscript.

Submitted: 8 July 2016

Revised: 30 November 2016

Accepted: 9 January 2017

References

- Abreu, C.M., R. Kumar, D. Hamilton, A.W. Dawdy, K. Creavin, S. Eivers, K. Finn, J.L. Balsbaugh, R. O'Connor, P.A. Kiely, et al. 2013. Site-specific phosphorylation of the DNA damage response mediator Rad9 by cyclin-dependent kinases regulates activation of checkpoint kinase 1. *PLoS Genet.* 9:e1003310. <http://dx.doi.org/10.1371/journal.pgen.1003310>
- Bastos de Oliveira, F.M., D. Kim, J.R. Cussiol, J. Das, M.C. Jeong, L. Doerfler, K.H. Schmidt, H. Yu, and M.B. Smolka. 2015. Phosphoproteomics reveals distinct modes of Mec1/ATR signaling during DNA replication. *Mol. Cell.* 57:1124–1132 (published erratum appears in *Mol. Cell.* 2015. 58:194). <http://dx.doi.org/10.1016/j.molcel.2015.01.043>
- Boos, D., L. Sanchez-Pulido, M. Rappas, L.H. Pearl, A.W. Oliver, C.P. Ponting, and J.F. Diffley. 2011. Regulation of DNA replication through Sld3-Dpb11 interaction is conserved from yeast to humans. *Curr. Biol.* 21:1152–1157. <http://dx.doi.org/10.1016/j.cub.2011.05.057>
- Bothmer, A., D.F. Robbiani, N. Feldhahn, A. Gazumyan, A. Nussenzweig, and M.C. Nussenzweig. 2010. 53BP1 regulates DNA resection and the choice between classical and alternative end joining during class switch recombination. *J. Exp. Med.* 207:855–865. <http://dx.doi.org/10.1084/jem.20100244>
- Bouwman, P., A. Aly, J.M. Escandell, M. Pieterse, J. Bartkova, H. van der Gulden, S. Hiddingh, M. Thanasoula, A. Kulkarni, Q. Yang, et al. 2010. 53BP1 loss rescues BRCA1 deficiency and is associated with triple-negative and BRCA-mutated breast cancers. *Nat. Struct. Mol. Biol.* 17:688–695. <http://dx.doi.org/10.1038/nsmb.1831>
- Bunting, S.F., E. Callén, N. Wong, H.T. Chen, F. Polato, A. Gunn, A. Bothmer, N. Feldhahn, O. Fernandez-Capetillo, L. Cao, et al. 2010. 53BP1 inhibits homologous recombination in *Brcal*-deficient cells by blocking resection

- of DNA breaks. *Cell*. 141:243–254. <http://dx.doi.org/10.1016/j.cell.2010.03.012>
- Callen, E., M. Di Virgilio, M.J. Kruhlak, M. Nieto-Soler, N. Wong, H.T. Chen, R.B. Faryabi, F. Polato, M. Santos, L.M. Starnes, et al. 2013. 53BP1 mediates productive and mutagenic DNA repair through distinct phosphoprotein interactions. *Cell*. 153:1266–1280. <http://dx.doi.org/10.1016/j.cell.2013.05.023>
- Cao, L., X. Xu, S.F. Bunting, J. Liu, R.H. Wang, L.L. Cao, J.J. Wu, T.N. Peng, J. Chen, A. Nussenzweig, et al. 2009. A selective requirement for 53BP1 in the biological response to genomic instability induced by Brca1 deficiency. *Mol. Cell*. 35:534–541. <http://dx.doi.org/10.1016/j.molcel.2009.06.037>
- Carr, A.M., and S. Lambert. 2013. Replication stress-induced genome instability: the dark side of replication maintenance by homologous recombination. *J. Mol. Biol.* 425:4733–4744. <http://dx.doi.org/10.1016/j.jmb.2013.04.023>
- Cescutti, R., S. Negrini, M. Kohzaki, and T.D. Halazonetis. 2010. TopBP1 functions with 53BP1 in the G1 DNA damage checkpoint. *EMBO J*. 29:3723–3732. <http://dx.doi.org/10.1038/emboj.2010.238>
- Chapman, J.R., A.J. Sossick, S.J. Boulton, and S.P. Jackson. 2012a. BRCA1-associated exclusion of 53BP1 from DNA damage sites underlies temporal control of DNA repair. *J. Cell Sci.* 125:3529–3534. <http://dx.doi.org/10.1242/jcs.105353>
- Chapman, J.R., M.R. Taylor, and S.J. Boulton. 2012b. Playing the end game: DNA double-strand break repair pathway choice. *Mol. Cell*. 47:497–510. <http://dx.doi.org/10.1016/j.molcel.2012.07.029>
- Chapman, J.R., P. Barral, J.B. Vannier, V. Borel, M. Steger, A. Tomas-Loba, A.A. Sartori, I.R. Adams, F.D. Batista, and S.J. Boulton. 2013. RIF1 is essential for 53BP1-dependent nonhomologous end joining and suppression of DNA double-strand break resection. *Mol. Cell*. 49:858–871. <http://dx.doi.org/10.1016/j.molcel.2013.01.002>
- Chen, X., D. Cui, A. Papusha, X. Zhang, C.D. Chu, J. Tang, K. Chen, X. Pan, and G. Ira. 2012. The Fun30 nucleosome remodeler promotes resection of DNA double-strand break ends. *Nature*. 489:576–580. <http://dx.doi.org/10.1038/nature11355>
- Chin, J.K., V.I. Bashkurov, W.D. Heyer, and F.E. Romesberg. 2006. Esc4/Rtt107 and the control of recombination during replication. *DNA Repair (Amst.)*. 5:618–628. <http://dx.doi.org/10.1016/j.dnarep.2006.02.005>
- Cho, Y.W., S. Hong, Q. Jin, L. Wang, J.E. Lee, O. Gavrilova, and K. Ge. 2009. Histone methylation regulator PTIP is required for PPAR γ and C/EBP α expression and adipogenesis. *Cell Metab.* 10:27–39. <http://dx.doi.org/10.1016/j.cmet.2009.05.010>
- Choi, J.H., L.A. Lindsey-Boltz, and A. Sancar. 2009. Cooperative activation of the ATR checkpoint kinase by TopBP1 and damaged DNA. *Nucleic Acids Res.* 37:1501–1509. <http://dx.doi.org/10.1093/nar/gkn1075>
- Clerici, M., D. Mantiero, G. Lucchini, and M.P. Longhese. 2005. The *Saccharomyces cerevisiae* Sae2 protein promotes resection and bridging of double strand break ends. *J. Biol. Chem.* 280:38631–38638. <http://dx.doi.org/10.1074/jbc.M508339200>
- Clerici, M., C. Trovesi, A. Galbiati, G. Lucchini, and M.P. Longhese. 2014. Mec1/ATR regulates the generation of single-stranded DNA that attenuates Tel1/ATM signaling at DNA ends. *EMBO J*. 33:198–216.
- Cussiol, J.R., C.M. Jablonowski, A. Yimit, G.W. Brown, and M.B. Smolka. 2015. Dampening DNA damage checkpoint signalling via coordinated BRCT domain interactions. *EMBO J*. 34:1704–1717. <http://dx.doi.org/10.15252/embj.201490834>
- Danielsen, J.M., D.H. Larsen, K.B. Schou, R. Freire, J. Falck, J. Bartek, and J. Lukas. 2009. HCLK2 is required for activity of the DNA damage response kinase ATR. *J. Biol. Chem.* 284:4140–4147. <http://dx.doi.org/10.1074/jbc.M808174200>
- Deng, C.X., and R.H. Wang. 2003. Roles of BRCA1 in DNA damage repair: a link between development and cancer. *Hum. Mol. Genet.* 12:R113–R123. <http://dx.doi.org/10.1093/hmg/ddg082>
- Dibitetto, D., M. Ferrari, C.C. Rawal, A. Balint, T. Kim, Z. Zhang, M.B. Smolka, G.W. Brown, F. Marini, and A. Pelliccioli. 2016. Slx4 and Rtt107 control checkpoint signalling and DNA resection at double-strand breaks. *Nucleic Acids Res.* 44:669–682. <http://dx.doi.org/10.1093/nar/gkv1080>
- Di Virgilio, M., E. Callen, A. Yamane, W. Zhang, M. Jankovic, A.D. Gitlin, N. Feldhahn, W. Resch, T.Y. Oliveira, B.T. Chait, et al. 2013. Rif1 prevents resection of DNA breaks and promotes immunoglobulin class switching. *Science*. 339:711–715. <http://dx.doi.org/10.1126/science.1230624>
- Escribano-Díaz, C., A. Orthwein, A. Fradet-Turcotte, M. Xing, J.T. Young, J. Tkáč, M.A. Cook, A.P. Rosebrock, M. Munro, M.D. Canny, et al. 2013. A cell cycle-dependent regulatory circuit composed of 53BP1-RIF1 and BRCA1-CtIP controls DNA repair pathway choice. *Mol. Cell*. 49:872–883. <http://dx.doi.org/10.1016/j.molcel.2013.01.001>
- Feng, L., K.W. Fong, J. Wang, W. Wang, and J. Chen. 2013. RIF1 counteracts BRCA1-mediated end resection during DNA repair. *J. Biol. Chem.* 288:11135–11143. <http://dx.doi.org/10.1074/jbc.M113.457440>
- Ferrari, M., D. Dibitetto, G. De Gregorio, V.V. Eapen, C.C. Rawal, F. Lazzaro, M. Tsabar, F. Marini, J.E. Haber, and A. Pelliccioli. 2015. Functional interplay between the 53BP1-ortholog Rad9 and the Mre11 complex regulates resection, end-tethering and repair of a double-strand break. *PLoS Genet.* 11:e1004928. <http://dx.doi.org/10.1371/journal.pgen.1004928>
- Fradet-Turcotte, A., M.D. Canny, C. Escribano-Díaz, A. Orthwein, C.C. Leung, H. Huang, M.C. Landry, J. Kitevski-LeBlanc, S.M. Noordermeer, F. Sicheri, and D. Durocher. 2013. 53BP1 is a reader of the DNA-damage-induced H2A Lys 15 ubiquitin mark. *Nature*. 499:50–54. <http://dx.doi.org/10.1038/nature12318>
- Fricke, W.M., and S.J. Brill. 2003. Slx1-Slx4 is a second structure-specific endonuclease functionally redundant with Sgs1-Top3. *Genes Dev.* 17:1768–1778. <http://dx.doi.org/10.1101/gad.1105203>
- Gaillard, H., T. García-Muse, and A. Aguilera. 2015. Replication stress and cancer. *Nat. Rev. Cancer*. 15:276–289. <http://dx.doi.org/10.1038/nrc3916>
- Gelot, C., I. Magdalou, and B.S. Lopez. 2015. Replication stress in mammalian cells and its consequences for mitosis. *Genes (Basel)*. 6:267–298.
- Germann, S.M., V.H. Oestergaard, C. Haas, P. Salis, A. Motegi, and M. Lisby. 2011. Dpb11/TopBP1 plays distinct roles in DNA replication, checkpoint response and homologous recombination. *DNA Repair (Amst.)*. 10:210–224. <http://dx.doi.org/10.1016/j.dnarep.2010.11.001>
- Gobbini, E., M. Villa, M. Gnugnoli, L. Menin, M. Clerici, and M.P. Longhese. 2015. Sae2 function at DNA double-strand breaks is bypassed by dampening Tel1 or Rad53 activity. *PLoS Genet.* 11:e1005685. <http://dx.doi.org/10.1371/journal.pgen.1005685>
- Granata, M., F. Lazzaro, D. Novarina, D. Panigada, F. Puddu, C.M. Abreu, R. Kumar, M. Grenon, N.F. Lowndes, P. Plevani, and M. Muzi-Falconi. 2010. Dynamics of Rad9 chromatin binding and checkpoint function are mediated by its dimerization and are cell cycle-regulated by CDK1 activity. *PLoS Genet.* 6:e1001047 (published erratum appears in *PLoS Genet.* 2014. 10:e1004535). <http://dx.doi.org/10.1371/journal.pgen.1001047>
- Greenberg, R.A., B. Soghian, S. Pathania, S.B. Cantor, Y. Nakatani, and D.M. Livingston. 2006. Multifactorial contributions to an acute DNA damage response by BRCA1/BARD1-containing complexes. *Genes Dev.* 20:34–46. <http://dx.doi.org/10.1101/gad.1381306>
- Gritenaite, D., L.N. Princz, B. Szakal, S.C. Bantele, L. Wendeler, S. Schilbach, B.H. Habermann, J. Matos, M. Lisby, D. Branzei, and B. Pfander. 2014. A cell cycle-regulated Slx4-Dpb11 complex promotes the resolution of DNA repair intermediates linked to stalled replication. *Genes Dev.* 28:1604–1619. <http://dx.doi.org/10.1101/gad.240515.114>
- Gunn, A., and J.M. Stark. 2012. I-SceI-based assays to examine distinct repair outcomes of mammalian chromosomal double strand breaks. *Methods Mol. Biol.* 920:379–391. http://dx.doi.org/10.1007/978-1-61779-998-3_27
- Heyer, W.D. 2015. Regulation of recombination and genomic maintenance. *Cold Spring Harb. Perspect. Biol.* 7:a016501. <http://dx.doi.org/10.1101/cshperspect.a016501>
- Iacovoni, J.S., P. Caron, I. Lassadi, E. Nicolas, L. Massip, D. Trouche, and G. Legube. 2010. High-resolution profiling of γ H2AX around DNA double strand breaks in the mammalian genome. *EMBO J*. 29:1446–1457. <http://dx.doi.org/10.1038/emboj.2010.38>
- Kakarougkas, A., A. Ismail, Y. Katsuki, R. Freire, A. Shibata, and P.A. Jeggo. 2013. Co-operation of BRCA1 and POH1 relieves the barriers posed by 53BP1 and RAP80 to resection. *Nucleic Acids Res.* 41:10298–10311. <http://dx.doi.org/10.1093/nar/gkt802>
- Kolodner, R.D., C.D. Putnam, and K. Myung. 2002. Maintenance of genome stability in *Saccharomyces cerevisiae*. *Science*. 297:552–557. <http://dx.doi.org/10.1126/science.1075277>
- Kumar, R., and C.F. Cheok. 2014. RIF1: a novel regulatory factor for DNA replication and DNA damage response signaling. *DNA Repair (Amst.)*. 15:54–59. <http://dx.doi.org/10.1016/j.dnarep.2013.12.004>
- Lazzaro, F., V. Sapountzi, M. Granata, A. Pelliccioli, M. Vaze, J.E. Haber, P. Plevani, D. Lydall, and M. Muzi-Falconi. 2008. Histone methyltransferase Dot1 and Rad9 inhibit single-stranded DNA accumulation at DSBs and uncapped telomeres. *EMBO J*. 27:1502–1512.
- Lee, S.E., J.K. Moore, A. Holmes, K. Umezū, R.D. Kolodner, and J.E. Haber. 1998. *Saccharomyces* Ku70, mre11/rad50 and RPA proteins regulate adaptation to G2/M arrest after DNA damage. *Cell*. 94:399–409. [http://dx.doi.org/10.1016/S0092-8674\(00\)81482-8](http://dx.doi.org/10.1016/S0092-8674(00)81482-8)
- Liu, Y., and M.B. Smolka. 2016. TOPBP1 takes RADical command in recombinational DNA repair. *J. Cell Biol.* 212:263–266. <http://dx.doi.org/10.1083/jcb.201601028>

- Manke, I.A., D.M. Lowery, A. Nguyen, and M.B. Yaffe. 2003. BRCT repeats as phosphopeptide-binding modules involved in protein targeting. *Science*. 302:636–639. <http://dx.doi.org/10.1126/science.1088877>
- Morin, I., H.P. Ngo, A. Greenall, M.K. Zubko, N. Morrice, and D. Lydall. 2008. Checkpoint-dependent phosphorylation of Exo1 modulates the DNA damage response. *EMBO J*. 27:2400–2410. <http://dx.doi.org/10.1038/emboj.2008.171>
- Morishima, K., S. Sakamoto, J. Kobayashi, H. Izumi, T. Suda, Y. Matsumoto, H. Tauchi, H. Ide, K. Komatsu, and S. Matsuura. 2007. TopBP1 associates with NBS1 and is involved in homologous recombination repair. *Biochem. Biophys. Res. Commun.* 362:872–879. <http://dx.doi.org/10.1016/j.bbrc.2007.08.086>
- Moudry, P., K. Watanabe, K.M. Wolanin, J. Bartkova, I.E. Wassing, S. Watanabe, R. Strauss, R. Troelsgaard Pedersen, V.H. Oestergaard, M. Lisby, et al. 2016. TOPBP1 regulates RAD51 phosphorylation and chromatin loading and determines PARP inhibitor sensitivity. *J. Cell Biol.* 212:281–288. <http://dx.doi.org/10.1083/jcb.201507042>
- Munoz, I.M., P.A. Jowsey, R. Toth, and J. Rouse. 2007. Phospho-epitope binding by the BRCT domains of hPTIP controls multiple aspects of the cellular response to DNA damage. *Nucleic Acids Res.* 35:5312–5322. <http://dx.doi.org/10.1093/nar/gkm493>
- Navadgi-Patil, V.M., and P.M. Burgers. 2008. Yeast DNA replication protein Dpb11 activates the Mec1/ATR checkpoint kinase. *J. Biol. Chem.* 283:35853–35859. <https://doi.org/10.1074/jbc.M807435200>
- Ohouo, P.Y., F.M. Bastos de Oliveira, B.S. Almeida, and M.B. Smolka. 2010. DNA damage signaling recruits the Rtt107-Slx4 scaffolds via Dpb11 to mediate replication stress response. *Mol. Cell.* 39:300–306. <http://dx.doi.org/10.1016/j.molcel.2010.06.019>
- Ohouo, P.Y., F.M. Bastos de Oliveira, Y. Liu, C.J. Ma, and M.B. Smolka. 2013. DNA-repair scaffolds dampen checkpoint signalling by counteracting the adaptor Rad9. *Nature*. 493:120–124. <http://dx.doi.org/10.1038/nature11658>
- Orthwein, A., S.M. Noordermeer, M.D. Wilson, S. Landry, R.I. Enchev, A. Sherker, M. Munro, J. Pinder, J. Salsman, G. Dellaire, et al. 2015. A mechanism for the suppression of homologous recombination in G1 cells. *Nature*. 528:422–426. <http://dx.doi.org/10.1038/nature16142>
- Pfander, B., and J.F. Diffley. 2011. Dpb11 coordinates Mec1 kinase activation with cell cycle-regulated Rad9 recruitment. *EMBO J*. 30:4897–4907. <http://dx.doi.org/10.1038/emboj.2011.345>
- Pierce, A.J., R.D. Johnson, L.H. Thompson, and M. Jasin. 1999. XRCC3 promotes homology-directed repair of DNA damage in mammalian cells. *Genes Dev.* 13:2633–2638. <http://dx.doi.org/10.1101/gad.13.20.2633>
- Prakash, R., Y. Zhang, W. Feng, and M. Jasin. 2015. Homologous recombination and human health: the roles of BRCA1, BRCA2, and associated proteins. *Cold Spring Harb. Perspect. Biol.* 7:a016600. <http://dx.doi.org/10.1101/cshperspect.a016600>
- Puddu, F., M. Granata, L. Di Nola, A. Balestrini, G. Piergiovanni, F. Lazzaro, M. Giannattasio, P. Plevani, and M. Muzi-Falconi. 2008. Phosphorylation of the budding yeast 9-1-1 complex is required for Dpb11 function in the full activation of the UV-induced DNA damage checkpoint. *Mol. Cell. Biol.* 28:4782–4793. <http://dx.doi.org/10.1128/MCB.00330-08>
- Roberts, T.M., M.S. Kobor, S.A. Bastin-Shanower, M. Ii, S.A. Horte, J.W. Gin, A. Emili, J. Rine, S.J. Brill, and G.W. Brown. 2006. Slx4 regulates DNA damage checkpoint-dependent phosphorylation of the BRCT domain protein Rtt107/Esc4. *Mol. Biol. Cell.* 17:539–548. <http://dx.doi.org/10.1091/mbc.E05-08-0785>
- Rodriguez, M., X. Yu, J. Chen, and Z. Songyang. 2003. Phosphopeptide binding specificities of BRCA1 COOH-terminal (BRCT) domains. *J. Biol. Chem.* 278:52914–52918. <http://dx.doi.org/10.1074/jbc.C300407200>
- Schwartz, E.K., and W.D. Heyer. 2011. Processing of joint molecule intermediates by structure-selective endonucleases during homologous recombination in eukaryotes. *Chromosoma*. 120:109–127. <http://dx.doi.org/10.1007/s00412-010-0304-7>
- Segurado, M., and J.F. Diffley. 2008. Separate roles for the DNA damage checkpoint protein kinases in stabilizing DNA replication forks. *Genes Dev.* 22:1816–1827. <http://dx.doi.org/10.1101/gad.477208>
- Tak, Y.S., Y. Tanaka, S. Endo, Y. Kamimura, and H. Araki. 2006. A CDK-catalysed regulatory phosphorylation for formation of the DNA replication complex Sld2-Dpb11. *EMBO J*. 25:1987–1996. <http://dx.doi.org/10.1038/sj.emboj.7601075>
- Tanaka, S., T. Umemori, K. Hirai, S. Muramatsu, Y. Kamimura, and H. Araki. 2007. CDK-dependent phosphorylation of Sld2 and Sld3 initiates DNA replication in budding yeast. *Nature*. 445:328–332. <http://dx.doi.org/10.1038/nature05465>
- Tang, J., N.W. Cho, G. Cui, E.M. Manion, N.M. Shanbhag, M.V. Botuyan, G. Mer, and R.A. Greenberg. 2013. Acetylation limits 53BP1 association with damaged chromatin to promote homologous recombination. *Nat. Struct. Mol. Biol.* 20:317–325. <http://dx.doi.org/10.1038/nsmb.2499>
- Vaze, M.B., A. Pelliccioli, S.E. Lee, G. Ira, G. Liberi, A. Arbel-Eden, M. Foiani, and J.E. Haber. 2002. Recovery from checkpoint-mediated arrest after repair of a double-strand break requires Srs2 helicase. *Mol. Cell.* 10:373–385. [http://dx.doi.org/10.1016/S1097-2765\(02\)00593-2](http://dx.doi.org/10.1016/S1097-2765(02)00593-2)
- Wang, G., X. Tong, S. Weng, and H. Zhou. 2012. Multiple phosphorylation of Rad9 by CDK is required for DNA damage checkpoint activation. *Cell Cycle*. 11:3792–3800. <http://dx.doi.org/10.4161/cc.21987>
- White, C.I., and J.E. Haber. 1990. Intermediates of recombination during mating type switching in *Saccharomyces cerevisiae*. *EMBO J*. 9:663–673.
- Yamane, K., X. Wu, and J. Chen. 2002. A DNA damage-regulated BRCT-containing protein, TopBP1, is required for cell survival. *Mol. Cell. Biol.* 22:555–566. <http://dx.doi.org/10.1128/MCB.22.2.555-566.2002>
- Yoo, H.Y., A. Kumagai, A. Shevchenko, A. Shevchenko, and W.G. Dunphy. 2009. The Mre11-Rad50-Nbs1 complex mediates activation of TopBP1 by ATM. *Mol. Biol. Cell.* 20:2351–2360. <http://dx.doi.org/10.1091/mbc.E08-12-1190>
- Yu, X., C.C. Chini, M. He, G. Mer, and J. Chen. 2003. The BRCT domain is a phospho-protein binding domain. *Science*. 302:639–642. <http://dx.doi.org/10.1126/science.1088753>
- Zegerman, P., and J.F. Diffley. 2007. Phosphorylation of Sld2 and Sld3 by cyclin-dependent kinases promotes DNA replication in budding yeast. *Nature*. 445:281–285. <http://dx.doi.org/10.1038/nature05432>
- Zhang, H., H. Liu, Y. Chen, X. Yang, P. Wang, T. Liu, M. Deng, B. Qin, C. Correia, S. Lee, et al. 2016. A cell cycle-dependent BRCA1-UHRF1 cascade regulates DNA double-strand break repair pathway choice. *Nat. Commun.* 7:10201. <http://dx.doi.org/10.1038/ncomms10201>
- Zhou, Y., P. Caron, G. Legube, and T.T. Paull. 2014. Quantitation of DNA double-strand break resection intermediates in human cells. *Nucleic Acids Res.* 42:e19. <http://dx.doi.org/10.1093/nar/gkt1309>
- Zierhut, C., and J.F. Diffley. 2008. Break dosage, cell cycle stage and DNA replication influence DNA double strand break response. *EMBO J*. 27:1875–1885. <http://dx.doi.org/10.1038/emboj.2008.111>
- Zimmermann, M., F. Lottersberger, S.B. Buonomo, A. Sfeir, and T. de Lange. 2013. 53BP1 regulates DSB repair using Rif1 to control 5' end resection. *Science*. 339:700–704. <http://dx.doi.org/10.1126/science.1231573>